HABITABLE ZONES AROUND MAIN-SEQUENCE STARS: NEW ESTIMATES

Ravi Kumar Kopparapu[1,2,3,4], Ramses Ramirez[1,2,3,4], James F. Kasting[1,2,3,4], Vincent Eymet[5],
Tyler D. Robinson[2,6,7], Suvrath Mahadevan[4,8], Ryan C. Terrien[4,8], Shawn Domagal-Goldman[2,9],
Victoria Meadows[2,6], and Rohit Deshpande[4,8]

[1] Department of Geosciences, Penn State University, 443 Deike Building, University Park, PA 16802, USA
[2] NASA Astrobiology Institute's Virtual Planetary Laboratory
[3] Penn State Astrobiology Research Center, 2217 Earth and Engineering Sciences Building, University Park, PA 16802, USA
[4] Center for Exoplanets & Habitable Worlds, The Pennsylvania State University, University Park, PA 16802, USA
[5] Laboratoire d'Astrophysique de Bordeaux, Universite de Bordeaux 1, UMR 5804, F-33270 Floirac, France
[6] Astronomy Department, University of Washington, Box 351580, Seattle, WA 98195-1580, USA
[7] University of Washington Astrobiology Program
[8] Department of Astronomy & Astrophysics, The Pennsylvania State University, 525 Davey Laboratory, University Park, PA 16802, USA
[9] Planetary Environments Laboratory, NASA Goddard Space Flight Center, Greenbelt, MD, USA

ABSTRACT

Identifying terrestrial planets in the habitable zones (HZs) of other stars is one of the primary goals of ongoing radial velocity (RV) and transit exoplanet surveys and proposed future space missions. Most current estimates of the boundaries of the HZ are based on one-dimensional (1D), cloud-free, climate model calculations by Kasting et al. However, this model used band models that were based on older HITRAN and HITEMP line-by-line databases. The inner edge of the HZ in the Kasting et al. model was determined by loss of water, and the outer edge was determined by the maximum greenhouse provided by a CO_2 atmosphere. A conservative estimate for the width of the HZ from this model in our solar system is 0.95–1.67 AU. Here an updated 1D radiative–convective, cloud-free climate model is used to obtain new estimates for HZ widths around F, G, K, and M stars. New H_2O and CO_2 absorption coefficients, derived from the HITRAN 2008 and HITEMP 2010 line-by-line databases, are important improvements to the climate model. According to the new model, the water-loss (inner HZ) and maximum greenhouse (outer HZ) limits for our solar system are at 0.99 and 1.70 AU, respectively, suggesting that the present Earth lies near the inner edge. Additional calculations are performed for stars with effective temperatures between 2600 and 7200 K, and the results are presented in parametric form, making them easy to apply to actual stars. The new model indicates that, near the inner edge of the HZ, there is no clear distinction between runaway greenhouse and water-loss limits for stars with $T_{eff} \lesssim 5000$ K, which has implications for ongoing planet searches around K and M stars. To assess the potential habitability of extrasolar terrestrial planets, we propose using stellar flux incident on a planet rather than equilibrium temperature. This removes the dependence on planetary (Bond) albedo, which varies depending on the host star's spectral type. We suggest that conservative estimates of the HZ (water-loss and maximum greenhouse limits) should be used for current RV surveys and *Kepler* mission to obtain a lower limit on $\eta_\oplus$, so that future flagship missions like *TPF-C* and *Darwin* are not undersized. Our model does not include the radiative effects of clouds; thus, the actual HZ boundaries may extend further in both directions than the estimates just given.

Key word: planetary systems

Online-only material: color figures, supplemental data (FITS) file (tar.gz)

1. INTRODUCTION

As of 2012 November, more than 800 extrasolar planetary systems have been detected,[10] and >2000 additional candidate systems from the *Kepler* mission are waiting to be confirmed (Batalha et al. 2012). One of the primary goals of the ongoing radial velocity (RV) and transit surveys is to identify a terrestrial mass planet (0.3–10 $M_\oplus$) in the so-called habitable zone (HZ), which is traditionally defined as the circumstellar region in which a terrestrial-mass planet with a CO_2–H_2O–N_2 atmosphere can sustain liquid water on its surface[11] (Huang 1959; Hart 1978; Kasting et al. 1993; Underwood et al. 2003; Selsis et al. 2007b; Kaltenegger & Sasselov 2011). Several potential HZ planet candidates have already been detected (Udry et al. 2007; Pepe

et al. 2011a; Borucki et al. 2011, 2012; Bonfils et al. 2011; Vogt et al. 2012; Tuomi et al. 2012), and it is expected that this number will greatly increase as time passes (Batalha et al. 2012). In the near future we may be able to study habitable planets orbiting nearby M stars. These planets are relatively close to their parent stars, leading to shorter orbital periods and an increase in the probability of a transit. NASA's *James Webb Space Telescope* (*JWST*), scheduled to launch in 2018, is considered to be marginally capable of obtaining a transit spectrum of an Earth-like planet orbiting a late M dwarf (Clampin et al. 2007; Kaltengger & Traub 2009; Deming et al. 2009). Several other surveys are either underway (Nutzman & Charbonneau 2008; MEARTH) or getting ready to be commissioned (Mahadevan et al. 2012; HPF) in an attempt to discover rocky planets in the HZs of low-mass stars.

The HZ limits that were cited in many recent discoveries were obtained from one-dimensional (1D) radiative–convective, cloud-free, climate model calculations by Kasting et al. (1993).

---

[10] exoplanets.org
[11] Abe et al. (2011) studied habitability of water-limited "land" planets and found that they could remain habitable much closer to their host stars.

For our Sun, these authors estimated the boundaries of the HZ to be 0.95 AU for the inner edge and 1.67 AU for the outer edge. These values represent the "water-loss" and "maximum greenhouse" limits, respectively. Other, less conservative limits for the inner edge are the "runaway greenhouse" and "recent Venus" limits. The latter estimate is empirical, based on the inference that Venus has not had liquid water on its surface for at least the past 1 billion years (Solomon & Head 1991). For the outer edge, there is a corresponding "early Mars" empirical estimate, based on the inference that Mars did have liquid water on its surface 3.8 billion years ago (the "first CO_2 condensation" limit of Kasting et al. 1993 should now be disregarded, as it has been shown that CO_2 clouds generally warm a planet's climate (Forget & Pierrehumbert 1997)). Some studies have investigated the effects of clouds on planetary emission spectra of Earth-like planets in a 1D model (Kitzmann et al. 2011a, 2011b), while others studied the habitability of specific systems, particularly Gl 581, in 1D (Wordsworth et al. 2010; Von Paris et al. 2011; Kaltenegger et al. 2011) and 3D (Wordsworth et al. 2011; Pierrehumbert 2011). Several other studies (Underwood et al. 2003; Selsis et al. 2007b) parameterized these results to estimate relationships between HZ boundaries and stellar parameters for stars of different spectral types.

Although these studies provided useful estimates of the HZ width, the Kasting et al. (1993) model has become outdated for several reasons.

1. Kasting et al. (1993) used "band models"[12] for H_2O and CO_2 absorption in the thermal-IR. These coefficients were considered valid up to ∼700 K. These coefficients were later replaced (Mischna et al. 2000) by coefficients generated using the correlated-k technique (Mlawer et al. 1997; Kato et al. 1999). A line-by-line (LBL) radiative transfer model, in this case LBLRTM (Clough & Iocono 1995), was used to generate detailed spectra for H_2O and CO_2 at a variety of different temperatures and pressures. Once the detailed spectra were calculated, separate broadband k-coefficients for both H_2O and CO_2 were generated by R. Freedman using standard procedures. But these coefficients were only derived for temperatures <350 K and should therefore underestimate thermal-IR absorption in warm, moist-greenhouse atmospheres. (This prediction was verified by direct experimentation with that model.) Furthermore, the coefficients adopted by Mischna et al. (2000) and used in subsequent climate modeling studies by the Kasting research group were obtained using the HITRAN 1996 database and had not been updated since then.

2. Recent studies (Halevy et al. 2009; Wordsworth et al. 2010) have pointed out that the Kasting et al. (1993) model may have significantly overestimated absorption of thermal-IR radiation by collision-induced absorption (CIA) bands of CO_2, which may affect the outer edge of the HZ (OHZ).

3. The Kasting et al. (1993) calculations spanned stellar effective temperatures from 7200 to 3700 K, corresponding approximately to stellar classes F0 to M0. Stellar effective temperature affects the HZ boundaries because the radiation from F stars is bluer relative to that from the Sun, whereas the radiation from K and M stars is redder, and this affects calculated planetary albedos. The HZ limits from the Kasting et al. (1993) model do not include M stars with effective temperatures lower than 3700 K. As pointed

out above, such stars are promising candidates for current observational surveys because their HZs are closer to the star. Therefore, potential rocky planets in the HZs will have shorter orbital periods and higher probability of transit.

In this paper, we address all the above major issues with the goal of deriving new, improved estimates for the boundaries of the HZ. The outline of the paper is as follows. In Section 2, we describe our 1D cloud-free climate model, corresponding model updates, and model validation with other studies. In Section 3, we present results from our climate model and discuss various HZ limits for our Earth. Section 4 presents HZ boundaries around F, G, K, and M spectral stellar spectral types and, then provides a generalized expression to calculate HZ boundaries and compares these boundaries with previous studies. We discuss the implications of these new results for currently known exoplanet planetary systems in Section 5 and present our conclusions in Section 6.

2. MODEL DESCRIPTION

We used a 1D, radiative–convective, cloud-free climate model based on Kasting (1988) for the inner edge of the HZ (IHZ) and Kasting (1991) for the OHZ calculations. Following Kasting et al. (1993), we assumed an Earth-mass planet with an H_2O (IHZ) or CO_2 (OHZ) dominated atmosphere for our base model. Sensitivity studies for different planetary masses are described in the following section. Both the inner and outer edge calculations relied on the so-called inverse climate modeling, in which the surface temperature is specified, and the model is used to calculate the corresponding solar flux needed to sustain it. To do this, the atmosphere was divided into 101 layers, and a specific pressure–temperature profile was assumed. For the inner edge, this consisted of a moist pseudoadiabat extending from the surface up to an isothermal (200 K) stratosphere. Methodology for calculating the pseudoadiabat was taken from Appendix A of Kasting (1988). The surface temperature was varied from 200 to 2200 K during the course of the calculations. For the outer edge, the surface temperature was fixed at 273 K, and the CO_2 partial pressure was varied from 1 to 37.8 bar (the saturation CO_2 partial pressure at that temperature). A moist H_2O adiabat was assumed in the lower troposphere, and a moist CO_2 adiabat was used in the upper troposphere when condensation was encountered, following the methodology in Appendix B of Kasting (1991).

H_2O and CO_2 clouds are neglected in the model, but the effect of the former is accounted for by increasing the surface albedo, as done in previous climate simulations by the Kasting research group (Kasting 1991; Haqq-Misra et al. 2008). It has been argued that this methodology tends to overestimate the greenhouse effect of dense CO_2 atmospheres (Goldblatt & Zahnle 2011). By contrast, our neglect of CO_2 clouds may cause us to underestimate the greenhouse effect of such atmospheres (Forget & Pierrehumbert 1997). Realistically determining the effects of clouds would require a 3D climate model, as most clouds form in updrafts, which are absent in 1D models. Some 1D climate modeling studies include partial cloud coverage (Selsis et al. 2007b) and/or a parameterized microphysical cloud model (Colaprete & Toon 2003; Zsom et al. 2012), but we do not consider them here because we cannot model them self-consistently in our model. The effects of clouds on the inner and outer edge boundaries are qualitatively understood, as discussed later in the paper. Testing these predictions quantitatively using 3D climate models should be a fruitful topic for future research.

---

[12] See Appendix B of Kasting (1988) for a detailed description of the band model.

Radiative transfer was handled by methods used in recent versions of the Kasting group climate model but with updated absorption coefficients (see next section). A δ two-stream approximation (Toon et al. 1989) was used to calculate the net absorbed solar radiation for each of the 101 layers, using separate eight-term, correlated-k coefficients for both CO_2 and H_2O to parameterize absorption in each of the 38 solar spectral intervals ranging from 0.2 to 4.5 μm. These terms are convolved with each other in each spectral interval, resulting in 64 separate radiative transfer calculations per interval. The solar flux was averaged over six zenith angles (11°0, 25°3, 39°6, 54°, 68°4, and 82°8) using Gaussian quadrature. The net outgoing IR radiation per layer was calculated using separate eight-term correlated-k coefficients for H_2O and CO_2 in 55 spectral intervals extending from 0 to 15,000 cm^{-1}. We used double gauss quadrature in place of a standard Gaussian scheme (Sykes 1952; Thomas & Stamnes 2002). Half of the k-coefficients are chosen within the g-space interval 0.95–1.00 for improved resolution of the steeply rising portion of the cumulative distribution function, yielding smoother stratospheric temperature behavior.

These coefficients also needed to be convolved with each other, as in the solar calculation. This produces $8 \times 8 \times 55 = 3520$ separate thermal-IR radiative transfer calculations at each time step in the climate model. This number is multiplied by a factor of six when we include CH_4 in the model, using six-term sums, and by another factor of six when we include C_2H_6. Thus, from a practical standpoint, the utility of this approach diminishes as the number of included greenhouse gases increases.

2.1. Model Updates

The following are the most significant updates to the climate model:

1. We have derived new k-coefficients (suggested to us by C. Goldblatt 2011, private communication) using a tool called KSPECTRUM. It is a program to produce high-resolution spectra of any gas mixture, in any thermodynamical conditions, from LBL databases such as HITRAN 2008 (Rothman et al. 2009) and HITEMP 2010 (Rothman et al. 2010). It is intended to produce reliable spectra, which can then be used to compute k-distribution data sets that may be used for subsequent radiative transfer analysis. The source code and a detailed description of the program are available at http://code.google.com/p/kspectrum/.

   We have produced two sets of coefficients, one using HITRAN 2008 and the other using the HITEMP 2010 database. For the HITRAN database we generated a matrix of eight-term absorption coefficients for both H_2O and CO_2, using KSPECTRUM, for the following range of pressures and temperatures: $p(\text{bar}) = [10^{-5}, 10^{-4}, 10^{-3}, 10^{-2}, 10^{-1}, 1, 10, 10^2]$ and $T(\text{K}) = [100, 150, 200, 250, 300, 350, 400, 600]$. In the case of HITEMP, eight-term absorption coefficients were derived only for H_2O, as our IHZ is H_2O dominated at high temperatures ($\geqslant$300 K) with only trace amounts of CO_2 (330 parts per million). The following grid was used to derive the H_2O HITEMP coefficients: $p(\text{bar}) = [10^{-1}, 1, 10, 10^2]$ and $T(\text{K}) = [350, 400, 600]$. The grid is condensed because of the high number of line transitions in the HITEMP database compared to HITRAN. The computational resources needed to derive absorption coefficients for the entire range of pressures and temperatures would be prohibitively large. Moreover, as discussed further below, we

justify the selection of this condensed grid by showing that the differences in coefficients generated from HITRAN and HITEMP become negligible below 350 K.

   In generating the k-coefficients, we have used different methodologies for CO_2 and H_2O. For CO2, we truncated the spectral lines at 500 cm^{-1} from the line center. Experimental evidence indicates that the absorption by CO_2 is overestimated if Lorentzian line shapes are used (Burch et al. 1969; Fukabori et al. 1986; Bezard et al. 1990; Halevy et al. 2009). Therefore, we used the prescription of Perrin & Hartmann (1989) for "sub-Lorentzian" absorption in the far wings of the lines when running KSPECTRUM. For H_2O, we truncated the spectral lines 25 cm^{-1} and overlaid a semi-empirical "continuum absorption." The Lorentz line shape is known to underestimate absorption for H_2O in the far wings (Halevy et al. 2009), possibly because of the tendency of H_2O to form dimers. The corresponding continuum absorption is therefore "super-Lorentzian" for H_2O, and we have used the "BPS" formalism of Paynter & Ramaswamy (2011) to parameterize this absorption.

2. We have included Rayleigh scattering by water vapor, as it can become important for wavelengths up to 1 μm (which is where the Wien peak occurs for low-mass stars). Rayleigh scattering by water was also considered by Kasting (1988) and Kasting et al. (1993), but these authors used the scattering coefficient for air because the coefficient for H_2O was not available, or at least not known to them. The following expression for the scattering cross section was adopted (Allen 1976; Vardavas & Carver 1984; Von Paris et al. 2010):

$$\sigma_{R, H_2O}(\lambda) = 4.577 \times 10^{-28} \left[\frac{6 + 3D}{6 - 7D} \right] \left[\frac{r}{\lambda} \right]^4 cm^2. \quad (1)$$

   Here D is the depolarization ratio (0.17 for H_2O; Marshall & Smith 1990); r is the wavelength (λ)-dependent refractive index, which is calculated as $r = 0.85 r_{\text{dryair}}$ (Edlén 1996); r_{dryair} is obtained from Equation (4) of Bucholtz (1995); and λ is in microns. Note that the coefficient in the Rayleigh scattering cross section given in Von Paris et al. (2010) should be seven orders of magnitude smaller, as shown in Equation (1). This is because the numerical factor 4.577×10^{-21} is applicable only if the coefficients A and B, defined in the Rayleigh scattering cross section (Vardavas & Carver 1984, Equation (26)), are factored into the wavelength dependence. By comparison, Selsis et al. (2007a) used an H_2O Rayleigh scattering cross section of 2.32×10^{-27} cm^2 at 0.6 μm. Evaluating Equation (1) at 0.6 μm gives a value of 2.5×10^{-27} cm^2, which is similar to the Selsis et al. (2007a) value.

3. Previous climate model calculations by our group and others (Kasting et al. 1984; Pollack et al. 1987; Kasting 1991; Forget & Pierrehumbert 1997; Mischna et al. 2000) parameterized collision-induced absorption (CIA) by CO_2 near 7 μm and beyond 20 μm by the formulation given in the Appendix of Kasting et al. (1984). This process is an important source of thermal-IR opacity in the types of dense, CO_2-rich atmospheres predicted to be found near the outer edge of the HZ. In our model we have updated CO_2-CIA using the parameterization described in Gruszka & Borysow (1997), Baranov et al. (2004), and Halevy et al. (2009).
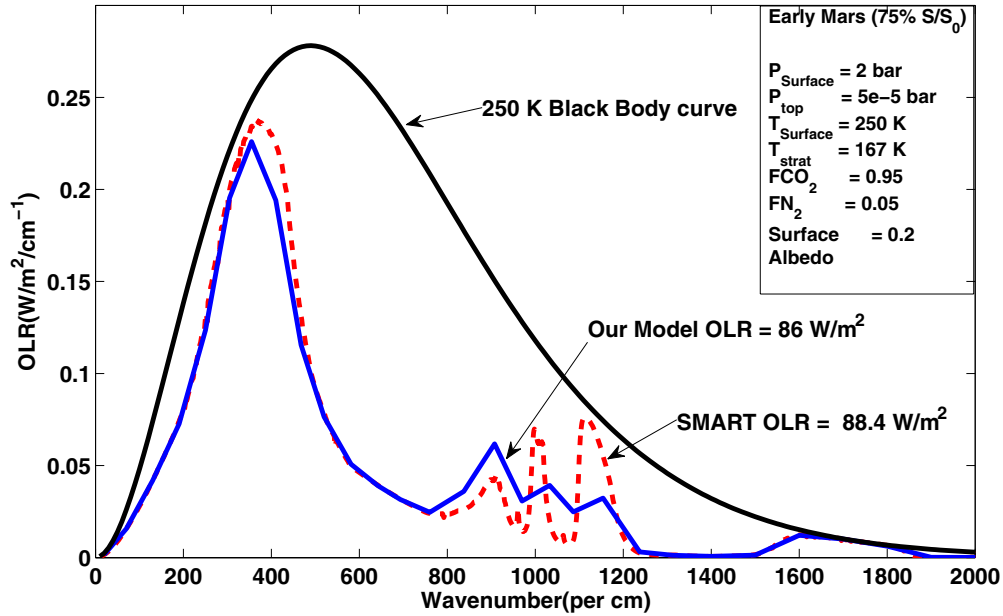
Figure 1. Plot of outgoing long-wave radiation vs. wavenumber for the 0–2000 cm^{-1} region comparing our OLR (blue solid curve) to that from SMART (red dashed curve). This calculation is for early Mars conditions, 2 bar CO_2, and constant stratospheric and surface temperatures of 167 and 250 K, respectively. The corresponding 250 K blackbody curve is shown in black. The integrated flux over all bands at the top of the atmosphere is 86 W m^{-2} for our model and 88.4 W m^{-2} for SMART.

(A color version of this figure is available in the online journal.)

4. The Shomate Equation[13] was used to calculate new heat capacity (c_p) relationships for CO_2 and H_2O. Notably, at low temperatures, the heat capacity for CO_2 decreased by ~30% relative to values in our previous model. This increased the dry adiabatic lapse rate, g/c_p, where g is gravity, by an equivalent amount but had surprisingly little effect on computed surface temperatures, apparently because the steeper lapse rate in the upper troposphere was largely compensated by a decrease in tropopause height. See Ramirez et al. (2013) for further details.

2.2. Model Validation

We have checked the accuracy of our climate model by comparing the output both with published results and with the 1D LBL radiative transfer model SMART (Spectral Mapping Atmospheric Radiative Transfer) developed by D. Crisp (Meadows & Crisp 1996; Crisp 1997). SMART is a well-tested model (Robinson et al. 2011) that accesses some of the same databases as does KSPECTRUM; however, its development and implementation are entirely independent. By comparing specific cases of interest with SMART, we can gain confidence that our calculated fluxes are correct, or at least that they are consistent with our assumptions about CO_2 and H_2O line shapes. For all our climate models that are compared with SMART, we used 70 atmospheric layers (we use 101 layers for all our HZ calculations). We could not use 101 layers in our flux comparisons due to numerical accuracy issues with SMART at high enough vertical resolution, although 70 layers produced a sufficiently accurate result with SMART.

2.2.1. Dense CO$_2$ Atmosphere

Dense CO_2-rich atmospheres have been suggested as warming agents for early Mars (Pollack et al. 1987; Kasting 1991;

Forget & Pierrehumbert 1997; Tian et al. 2010). Planets close to the OHZ may develop dense, CO_2-rich atmospheres as a consequence of outgassing from volcanism, which can only be balanced by surface weathering if the planet's surface temperature remains above freezing. The CO_2 feedback effect fails at some distance because CO_2 begins to condense out of the atmosphere, lowering the tropospheric lapse rate and reducing the greenhouse effect. CO_2 is also an effective Rayleigh scatterer (2.5 times better than air), and so a dense CO_2 atmosphere is predicted to have a high albedo, which offsets its greenhouse effect (Kasting 1991). The OHZ boundary can then be taken as this "maximum greenhouse limit" where Rayleigh scattering by CO_2 begins to outweigh the greenhouse effect.

Figure 1 shows net outgoing long-wave radiation (OLR) versus wavenumber in the range 0–2000 cm^{-1} for a Mars-mass planet with a 2 bar CO_2 atmosphere and a surface temperature of 250 K. The solar constant is assumed to be 75% of its present value (1360 W m^{-2}), matching the solar flux incident on early Mars (3.8 Gyr). The integrated flux over all bands at the top of the atmosphere from our model (86 W m^{-2}, blue solid curve) matches well with SMART (88.4 W m^{-2}, dashed red curve). Our model has a coarser spectral resolution than does SMART, and it appears that between 800 and 1200 cm^{-1} the differences could become important. But this is compensated by the fact that our OLR in these intervals can be considered as a running average of the OLR from SMART. Nevertheless, most of the difference in the OLR arises from significant absorption in the 667 cm^{-1} (15 m) vibrational band of CO_2, which is closer to the peak of the blackbody curve.

A similar study for early Mars conditions with a 2 bar CO_2 atmosphere was considered by Wordsworth et al. (2010). They have also used KSPECTRUM to derive their absorption coefficients and truncated the spectral lines at 500 cm^{-1} from the line center for CO_2, as done here. As our surface albedo for this calculation (0.2) is also the same, we can directly compare the results from both studies. Figure 2(c) from Wordsworth et al. (2010) shows that the net OLR from their model is
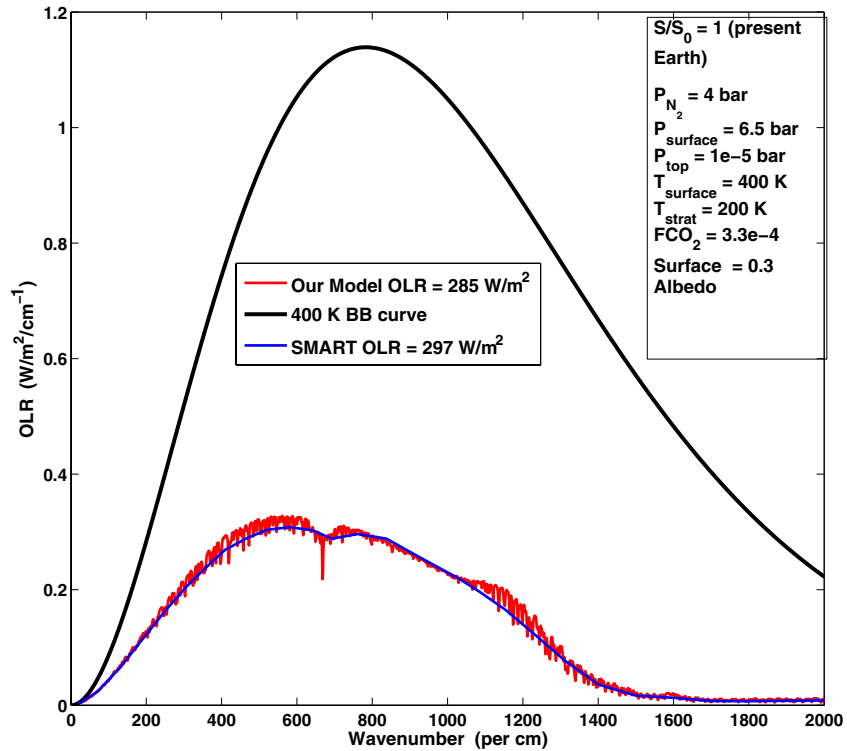

Figure 2. Plot of outgoing long-wave radiation vs. wavenumber for the 0–2000 cm^{-1} region comparing our OLR (blue solid curve) to that from SMART (red dashed curve). This calculation is for a dense H_2O atmosphere with stratospheric and surface temperatures of 200 and 400 K, respectively. The corresponding 400 K blackbody curve is shown in black. Both the models appear to be in good agreement. The integrated flux over all bands at the top of the atmosphere is 285 W m^{-2} for our model and 297 W m^{-2} for SMART, with differences possibly arising from different formalisms of continuum absorption (BPS vs. CKD; see the text for details).

(A color version of this figure is available in the online journal.)

88.17 W m^{-2} compared to our 86 W m^{-2}. The differences are due to the different number of atmospheric layers used in these models. Wordsworth et al. (2010) used 22 layers in their model, compared to 70 layers in our SMART comparison climate models. The number of vertical atmospheric layers used in the model affects the OLR because the Toon et al. (1989) algorithm, used in both models, assumes that each layer is isothermal. With few isothermal layers, more IR radiation is emitted from the upper part of each layer, which is a little hotter than it should be and has the smallest optical depth, as measured from the top of the atmosphere.[14]

2.2.2. Dense H_2O Atmosphere

The inner edge of the HZ in our model is determined by the so-called moist-greenhouse effect, in which the stratosphere becomes water dominated, leading to rapid escape of hydrogen to space. Figure 2 shows the net outgoing IR as a function of wavenumber for a dense H_2O atmosphere. Here we assumed an Earth-mass planet with a surface temperature of 400 K and a surface albedo of 0.3. The stratospheric temperature is assumed to be constant at 200 K. The stratosphere becomes tenuous at these high surface temperatures and has little effect on the outgoing IR flux. The background gas is 4 bar of N_2, and the total surface pressure is 6.5 bar (These conditions were assumed for specific intercomparison with SMART for this test case.) The flux incident at the top of the atmosphere is assumed to be the current solar flux at Earth's distance from the Sun.

As with the dense CO_2 case, in Figure 2 we compare our model (solid blue curve) with SMART (dashed red curve) for

the dense H_2O atmosphere. Although both model spectra appear to be in good agreement, the integrated flux over all bands at the top of the atmosphere from our model is 285 W m^{-2} compared to 297 W m^{-2} from SMART. The differences arise in the window region of the water vapor (800–1200 cm^{-1}) and also in between 300 and 600 cm^{-1}, where our model absorbs more than SMART. A possible reason is that we are using the BPS continuum, as opposed to the "CKD" continuum (Clough et al. 1989) used by SMART. The BPS formalism is based on empirical measurements that take into account the contribution of dimers, resulting in more absorption of outgoing IR radiation (see Paynter & Ramaswamy 2011, Table 3; Shine et al. 2012).

3. RESULTS

In the subsections that follow, we estimate HZ boundaries around a star similar to our Sun. We first compare results from our model using HITRAN and HITEMP databases, estimate HZ limits for non-Earth-like planets, and discuss the effect of clouds on the HZ boundaries.

3.1. Inner Edge of the HZ (IHZ)

The inner edge of the HZ is calculated by increasing the surface temperature of a fully saturated "Earth" model from 220 K up to 2200 K. The effective solar flux S_{eff}, which is the value of solar constant required to maintain a given surface temperature, is calculated from the ratio between the *net* outgoing IR flux F_{IR} and the *net* incident solar flux F_{SOL}, both evaluated at the top of the atmosphere. The total flux incident at the top of the atmosphere is taken to be the present solar constant at Earth's orbit 1360 W m^{-2}. The planetary albedo is calculated as the ratio between the upward and downward solar fluxes.

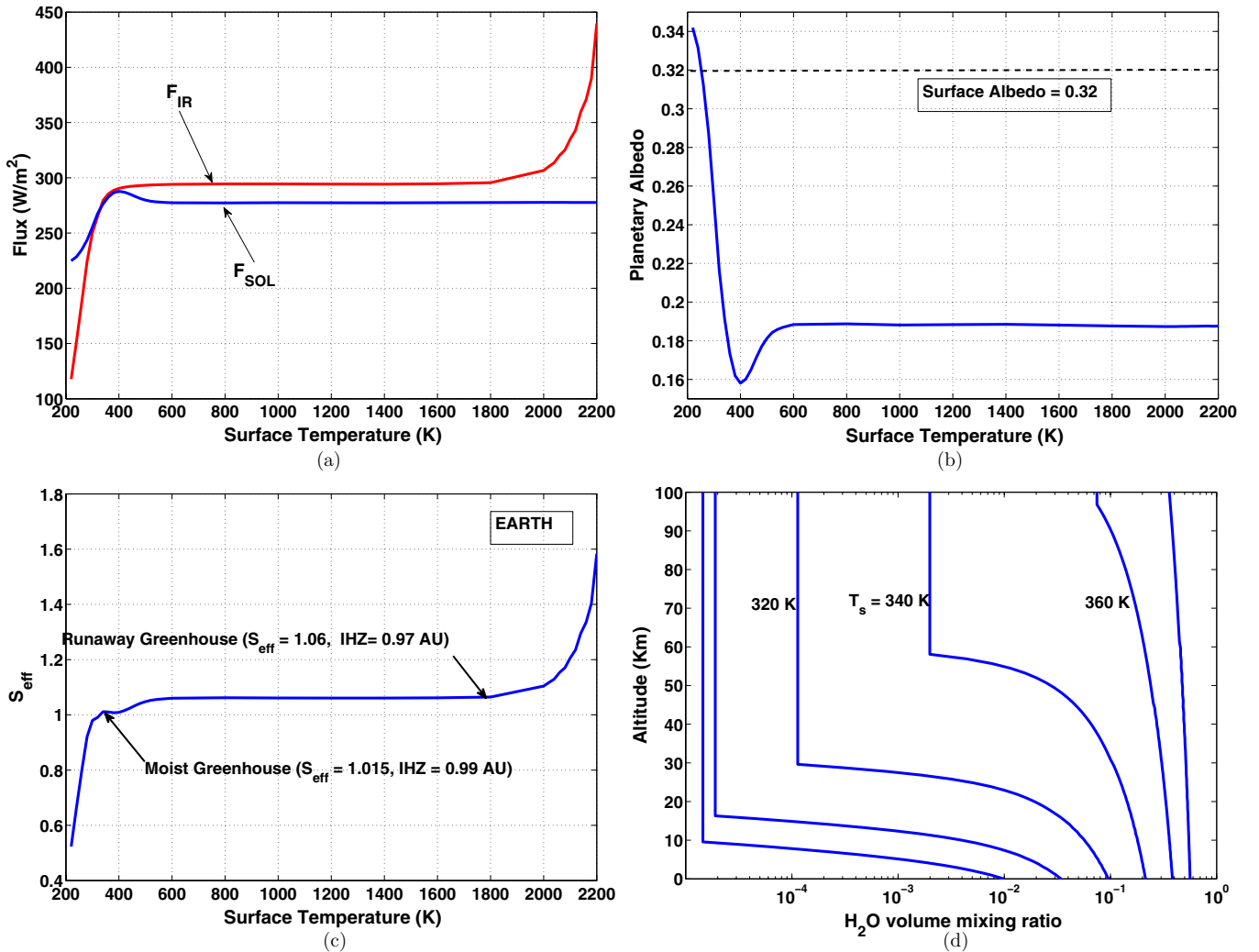[14] We ran our climate model with 22 layers and found that our OLR increased to 89.1 W m^{-2}.

Figure 3. Inner edge of the habitable zone calculations from our updated climate model. Various parameters are shown as a function of surface temperature: (a) net outgoing IR flux and net incident solar flux; (b) planetary albedo; (c) effective solar flux, $S_{eff} = F_{IR}/F_{SOL}$; and (d) water vapor profile. These calculations were performed with the HITEMP 2010 database. The water-loss (moist-greenhouse) limit, which is most relevant to habitability, is at 0.99 AU, and runaway greenhouse is at 0.97 AU. The corresponding estimates from the Kasting et al. (1993) climate model are 0.95 AU for the moist greenhouse and 0.84 AU for the runaway greenhouse.

(A color version of this figure is available in the online journal.)

The calculated radiative fluxes, planetary albedo, and water vapor profile for various surface temperatures are shown in Figure 3. Absorption coefficients derived from the HITEMP 2010 database, overlaid by the BPS formalism (Paynter & Ramaswamy 2011), were used in generating these results. Figure 3(a) shows that F_{IR} increases with surface temperature and then levels out at 291 W m^{-2}, as the atmosphere becomes opaque to IR radiation at all wavelengths.[15] Beyond 2000 K, F_{IR} increases again as the lower atmosphere and surface begin to radiate in the visible and near-IR (NIR), where the water vapor opacity is low. F_{SOL} initially increases as a consequence of absorption of NIR solar radiation by H_2O. It then decreases to a constant value (264 W m^{-2}) at higher temperatures as Rayleigh scattering becomes important. Planetary albedo (Figure 3(b)) provides an alternative way of understanding this behavior. It goes through a minimum at a surface temperature of 400 K, corresponding to the maximum in F_{SOL}, and then flattens out at a value of 0.193.

The inner edge of the HZ for our Sun can be calculated from Figure 3(c). The behavior of F_{IR} and F_{SOL} causes S_{eff} to increase initially and then remain constant at higher temperatures. Two limits for the IHZ boundary can be calculated. The first one is the "moist-greenhouse" (or water-loss) limit, which is encountered at a surface temperature of 340 K when $S_{eff} = 1.015$. At this limit, the water vapor content in the stratosphere increases dramatically, by more than an order of magnitude, as shown in Figure 3(d). This is the relevant IHZ boundary for habitability considerations, although it should be remembered that the actual inner edge may be closer to the Sun if cloud feedback tends to cool the planet's surface, as expected.[16] The orbital distance corresponding to the cloud-free water-loss limit is $d = 1/S_{eff}^{0.5} = 0.99$ AU for an Earth-like planet orbiting the Sun.

---

[15] This value of 291 W m^{-2} closely matches with the value from Figure 4.37 of Pierrehumbert (2010) for a planet saturated with pure water vapor atmosphere and with a surface gravity of 10 ms^{-2}.

[16] The total H_2O inventory assumed here is equal to the amount of water in Earth's oceans—1.4×10^{24} g. This amounts to 2×10^{28} atoms cm^{-2}. Once the stratosphere becomes wet, water vapor photolysis releases hydrogen, which can escape to space by the diffusion-limited escape rate. The timescale for water loss approaches the age of the Earth when the mixing ratio of water is $\sim 3 \times 10^{-3}$, which happens at a surface temperature of 340 K.
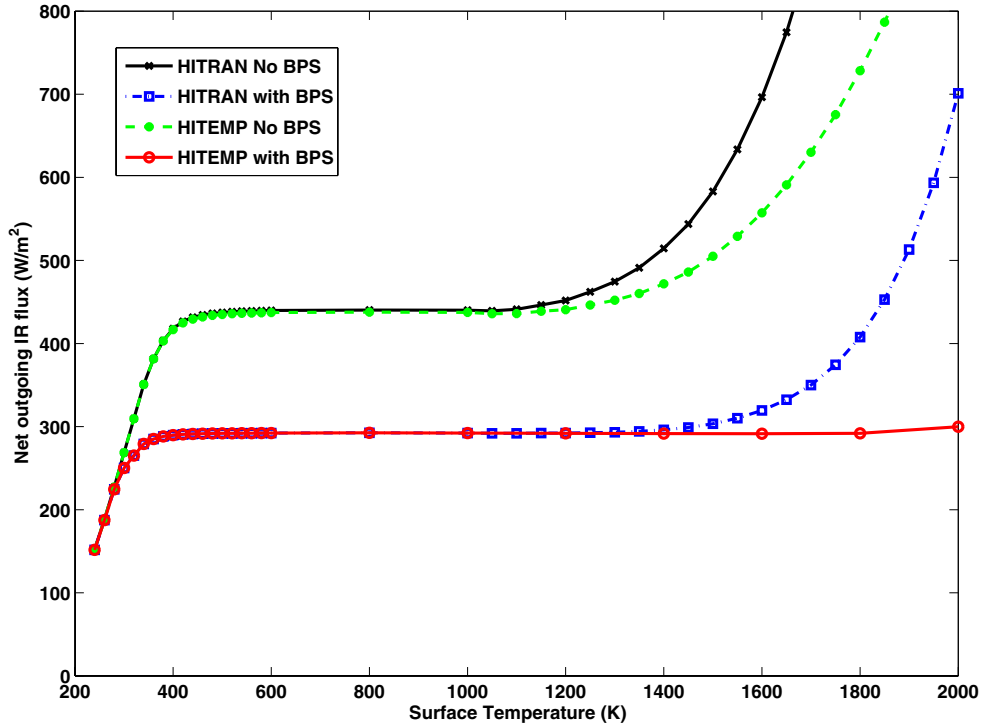
Figure 4. Comparison of outgoing IR radiation (F_{IR}) from HITEMP and HITRAN databases, with (blue and red curves) and without (black and green curves) continuum absorption. F_{IR} is lower in the "with BPS" case for both databases because the continuum absorption becomes significant in the water vapor window regions.

(A color version of this figure is available in the online journal.)

The second IHZ limit is the runaway greenhouse at which the oceans evaporate entirely. The limiting S_{eff} from Figure 3(c) is 1.06, which corresponds to a distance of 0.97 AU. Both calculated IHZ limits are significantly farther from the Sun than the values found by Kasting et al. (1993; 0.95 AU for the water-loss limit and 0.84 AU for the runaway greenhouse). The difference is caused by increased atmospheric absorption of incoming solar radiation by H_2O in the new model. As pointed out by Kasting et al. (1993), a third estimate for the IHZ boundary can be obtained from radar observations of Venus by the *Magellan* spacecraft, which suggest that liquid water has been absent from the surface of Venus for at least 1 Gyr (Solomon & Head 1991). The Sun at that time was ∼92% of the present-day luminosity, according to standard stellar evolutionary models (Baraffe et al. 1998; Bahcall et al. 2001; see Table 2). The current solar flux at Venus distance is 1.92 times that of Earth. Therefore, the solar flux received by Venus at that time was $0.92 \times 1.92 = 1.76$ times that of Earth. This empirical estimate of the IHZ edge corresponds to an orbital distance of $d = (1/1.76)^{0.5} = 0.75$ AU for the present day. Note that this distance is greater than Venus' orbital distance of 0.72 AU because the constraint of surface water was imposed at an earlier time in the planet's history.

3.2. Comparison of Inner Edge Results Using the HITEMP and HITRAN Databases

In Figure 4, we show F_{IR} as a function of surface temperature (similar to Figure 3(a)). We wish to compare the outgoing IR calculated from HITRAN and HITEMP databases with and without overlaying the continuum absorption. Figure 4 shows two significant differences as follows:

1. The limiting value of F_{IR} that leads to a runaway greenhouse happens at a much higher value (440 W m^{-2}; black

and green curves) when the BPS H_2O continuum formalism is not implemented, and at a lower F_{IR} (291 W m^{-2}; red and blue curves) when the BPS continuum is included in our model. The continuum is based on measurements of absorption in the water vapor window regions (i.e., 800–1200 cm^{-1} and 2000–3000 cm^{-1}). At high temperatures, the contribution of the continuum absorption in these window regions becomes significant, and this, in turn, decreases the outgoing IR flux.

2. The moist-greenhouse (water-loss) limit moves much closer to the Sun (to 0.87 AU) when continuum absorption is not included, as compared to 0.99 AU when it is included in our model. This is a direct consequence of the differences in F_{IR} described above. When F_{IR} increases with the continuum turned off, S_{eff} (ratio of F_{IR} to F_{SOL}) increases and the IHZ distance $d = 1/S_{eff}^{0.5}$ decreases. The result can be understood physically by noting that in the model where the continuum is absent, the planet needs more effective solar flux to maintain a given surface temperature because more thermal-IR radiation leaks away into space; hence, the IHZ boundary must move inward.

A similar change can be seen in the runaway greenhouse limit: the "No BPS" model transitions to runaway at a higher S_{eff} than does the "with BPS" model. The corresponding runaway greenhouse limit changes from 0.97 AU (with continuum absorption) to 0.76 AU (without continuum absorption). Figure 4 also shows that the upturn in F_{IR} beyond 800 K happens at lower surface temperatures when continuum absorption is not included. It should be remembered that this upturn in F_{IR} happens because, as the surface warms, the region in the troposphere over which the temperature profile follows a dry adiabat expands upward, while the moist convective layer in the upper
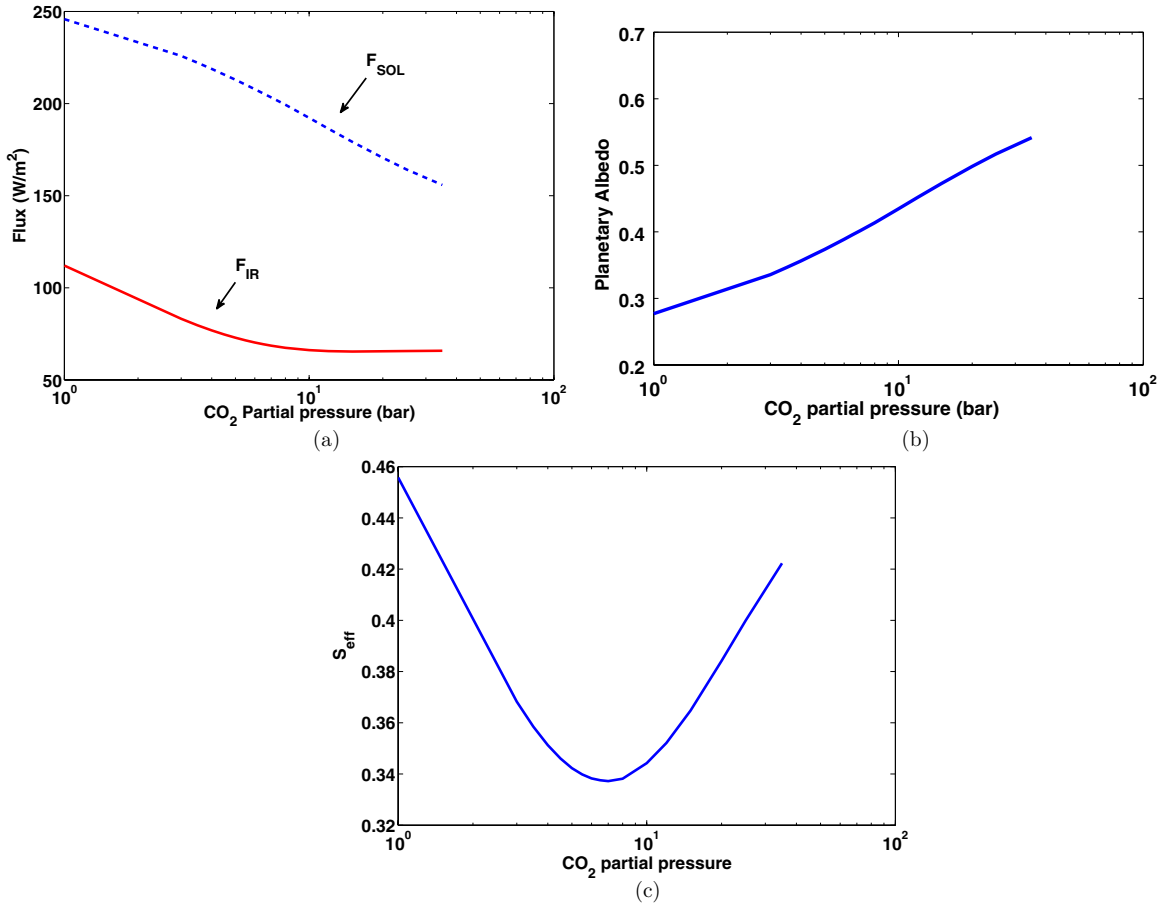
Figure 5. Outer edge of the habitable zone calculations from our climate model, shown as a function of CO_2 partial pressure, pCO_2: (a) net outgoing IR flux and net incident solar flux, (b) planetary albedo, and (c) effective solar flux. The maximum greenhouse limit, where the atmosphere becomes opaque to outgoing IR radiation, is at 1.70 AU ($S_{eff} = 0.343$). The previous estimate from the Kasting et al. (1993) climate model was 1.67 AU.

(A color version of this figure is available in the online journal.)

troposphere becomes thinner. Eventually, when the moist convective region (the cloud layer) begins thin enough, radiation emitted from the dry adiabatic portion of the atmosphere begins to escape to space. The dry adiabatic lapse rate is steeper than the moist adiabatic lapse rate by about a factor of 9 ($\sim$10 K km^{-1} versus 1.1 K km^{-1}); hence, the emitted radiation flux is much higher. This can be understood from the integrated form of Schwarzchild's equation, which shows that the emitted flux is proportional to the temperature gradient (see, e.g., Equation (A4) in Kasting et al. 1984). Unlike Kasting (1988), we find that the emitted flux increases at all thermal-IR wavelengths shorter than 4 μm. The amount of visible radiation emitted remains negligible for surface temperatures of 2200 K or below. Without the continuum there are fewer lines to cause absorption in these thermal-IR bands, and hence a lower temperature would suffice to cause the upturn. Figure 4 also shows that the model that includes both HITEMP and continuum (red curve) is the one that absorbs the most outgoing IR radiation (which is the one that was used to derive inner HZ limits in Section 3.1).

3.3. Outer Edge of the HZ (OHZ)

In determining the OHZ, the surface temperature of an Earth-like planet with 1 bar N$_2$ atmosphere was fixed at 273 K and the atmospheric CO_2 partial pressure, pCO_2, was varied from 1 to 35 bar (the saturation vapor pressure for CO_2 at that temperature). The stratospheric temperature was chosen as follows: The model atmosphere (Mars-like planet) in which the onset of CO_2 condensation occurs has a cold-trap temperature of 154 K at an altitude where the ratio of the saturation vapor pressure to the ambient pressure is unity. We replace the temperature profile above this altitude with a constant temperature of 154 K. This allows us to calculate the solar flux (S_{eff}) required to maintain a global mean surface temperature of 273 K as explained in Section 3.1. Our working hypothesis is that atmospheric CO_2 would accumulate as these planets cooled because of the negative feedback provided by the carbonate-silicate cycle. Results from our model calculations are shown in Figure 5.

The incident solar (F_{SOL}) and outgoing IR (F_{IR}) fluxes are shown in Figure 5(a). F_{IR} decreases initially as CO_2 partial pressure is increased; this is an indication of the greenhouse effect of CO_2. At $\sim$10 bar, F_{IR} asymptotically approaches a constant value as the atmosphere becomes optically thick at all IR wavelengths. F_{SOL} decreases monotonically with increases in CO_2 partial pressure as a result of increased Rayleigh scattering. Correspondingly, the planetary albedo increases to high values at large CO_2 partial pressures, as shown in Figure 5(b). The solar and IR fluxes, acting in opposite directions, create a minimum of $S_{eff} = 0.325$ at a CO_2 partial pressure of $\sim$8 bar (Figure 5(c)), corresponding to a distance $d = 1.70$ AU. This defines the maximum greenhouse limit on the OHZ. By

Table 1
Habitable Zone Distances around Our Sun from Our Updated 1D Climate Model

Model	Inner Habitable Zone			Outer Habitable Zone	
	Moist Greenhouse	Runaway Greenhouse	Recent Venus	Maximum Greenhouse	Early Mars
This paper	0.99 AU	0.97 AU	0.75 AU	1.70 AU	1.77 AU
Kasting et al. (1993)	0.95 AU	0.84 AU	0.75 AU	1.67 AU	1.77 AU

Notes. For comparison, estimates from Kasting et al. (1993) are also shown.

comparison, Kasting et al. (1993) model predicted $d = 1.67$ AU for the maximum greenhouse limit. As emphasized earlier, radiative warming by CO_2 clouds is neglected here, even though they should be present in this calculation. Therefore, our OHZ limit should be considered as a conservative estimate, that is, the real outer edge is probably farther out.

As with the inner edge model, a more optimistic empirical limit on the OHZ can be estimated based on the observation that early Mars was warm enough for liquid water to flow on its surface (Pollack et al. 1987; Bibring et al. 2006). Assuming that the dried-up riverbeds and valley networks on the Martian surface are 3.8 Gyr old, the solar luminosity at that time would have been ∼75% of the present value (see Equation (1) in Gough (1981) and Table 2 in Bahcall et al. (2001)). The present-day solar flux at Mars distance is 0.43 times that of Earth. Therefore, the solar flux received by Mars at 3.8 Gyr was $0.75 \times 0.43 = 0.32$ times that of Earth. The corresponding OHZ limit today, then, would be $d = (1/0.32)^{0.5} \approx 1.77$ AU.

Note that this distance exceeds the maximum greenhouse limit of 1.70 AU estimated above, indicating that to keep early Mars wet, additional greenhouse gases other than CO_2 and H_2O may be required. In fact, Ramirez et al. (2013) show that a 3 bar atmosphere containing 90% CO_2 and 10% H_2 could have raised the mean surface temperature of early Mars above the freezing point of water. The warming is caused by the collision-induced absorption due to foreign broadening by molecular hydrogen. It should be acknowledged that some authors (e.g., Segura et al. 2002, 2008) do not agree that early Mars must have been warm; however, in our view, these cold early Mars models do not produce enough rainfall to explain valley formation (Ramirez et al. 2013).

3.4. Effect of Clouds on the HZ Boundaries

We summarize various cloud-free HZ boundary estimates for Earth in Table 1. Although we updated our radiative transfer model to incorporate new absorption coefficients, this by itself may not yield a significantly better estimate for the width of the HZ. The reason is that it is widely acknowledged that the HZ boundaries will be strongly influenced by the presence of clouds. H_2O clouds should move the inner edge inward (Kasting 1988; Selsis et al. 2007b) because their contribution to a planet's albedo is expected to outweigh their contribution to the green-house effect. (A dense H_2O atmosphere is already optically thick throughout most of the thermal-IR, so adding clouds has only a small effect on the outgoing IR radiation.) Conversely, CO_2 ice clouds are expected to cause warming in a dense CO_2 atmosphere because they backscatter outgoing thermal-IR radiation more efficiently than they backscatter incoming visible/NIR radiation (Forget & Pierrehumbert 1997). One can demonstrate the nature of these cloud influences using 1D models, as was done in Selsis et al. (2007b). Making quantitative statements is difficult, however, because the warming or cooling effect of

Table 2
Habitable Zones around Our Sun for Different Planetary Parameters

Model	Inner Habitable Zone		Outer Habitable Zone
	Moist Greenhouse	Runaway Greenhouse	Maximum Greenhouse
Mars-sized planet[a]	1.035 AU	1.033 AU	1.72 AU
Earth	0.99 AU	0.97 AU	1.70 AU
Super-Earth[b]	0.94 AU	0.92 AU	1.67 AU
$pCO_2 = 5.2 \times 10^{-3}$ bar[c]	**1.00 AU**	**0.97 AU**	⋯
$pCO_2 = 5.2 \times 10^{-2}$ bar	1.02 AU	0.97 AU	⋯
$pCO_2 = 5.2 \times 10^{-1}$ bar	1.02 AU	0.97 AU	⋯
$pCO_2 = 5.2$ bar	0.99 AU	0.97 AU	⋯

Notes.
[a] Surface gravity $= 3.73$ m s^{-2}.
[b] Surface gravity $= 25$ m s^{-2}.
[c] $pCO_2 = 5.2 \times 10^{-4}$ bar for our standard Earth model. Note that these CO_2 pressures are not actual partial pressures; rather, they represent the surface pressure that would be produced if this amount of CO_2 were placed in the atmosphere by itself. The 330 ppmv of CO_2 in our standard 1 bar atmosphere would produce a surface pressure of 5.2×10^{-4} bar if the rest of the atmosphere was not present. When lighter gases such as N_2 and O_2 are present, they increase the atmospheric scale height and cause CO_2 to diffuse upward, thereby lowering its partial pressure at the surface.

clouds depends on a host of parameters, including their heights, optical depths, particle sizes, and, most importantly, fractional cloud coverage. Forget & Pierrehumbert (1997) obtained as much as 70° of warming out of an optical depth 10 CO_2 cloud with 100% cloud cover, but that warming dropped by 30° if fractional cloud cover was reduced to 75%. Realistic fractional cloud cover for condensation clouds is closer to 50%, because such clouds tend to form on updrafts, and approximately half the air in the troposphere is rising at any one time while the other half is descending.

The best way to incorporate cloud effects in a climate calculation is to use a 3D general circulation model (GCM). Attempts were made to explain warm early Mars using such 3D models (Forget et al. 2013), but none have yet succeeded. One can, however, do significantly better than in our 1D model, and so further research in this area is warranted (Abe et al. 2011; Wordsworth et al. 2011).

3.5. Habitable Zone Limits for Non-Earth-like Planets

In Table 2, we show the effect of surface gravities on the HZs of two planets. These planetary gravities were selected to encompass the mass range from Mars (gravity of 3.73 ms^{-2}) to a roughly 10 $M_\oplus$ super-Earth (gravity of 25 ms^{-2}). Both planets were assumed to have a 1 bar background N_2 atmosphere. This may be unrealistic because proportionately more nitrogen is put on the smaller planet than the larger one; however, this allows

direct comparison with Kasting et al. (1993). Table 2 shows that the habitability limits move slightly outward for a Mars-sized planet and inward for a super-Earth. This is because the column depth is larger for a Mars-sized planet, which increases the greenhouse effect (at the inner edge) and albedo (at the outer edge). Since the inner edge moves closer to the star for the super-Earth planet, while the outer edge changed little, we can conclude that, for a given surface pressure, larger planets have somewhat wider HZs than do small ones.

We also performed sensitivity tests on the inner edge of the HZ by varying the amount of atmospheric CO_2 (the outer edge calculation already factors in this change in CO_2). It is quite possible that some terrestrial planets may have varying amount of CO_2 because of different silicate weathering rates. As shown in Table 2, changes in pCO_2 would not change the runaway greenhouse limit, as it is reached in an H_2O-dominated atmosphere. The moist-greenhouse limit does change, as an increase in pCO_2 increases the surface temperature and hence facilitates water loss. The maximum destabilization occurs at a $pCO_2 = 5.2 \times 10^{-3}$ bar approximately 10 times the present terrestrial pCO_2 level (the critical distance, shown in bold in Table 2, is 1.00 AU).

This suggests that a 10-fold increase in CO_2 concentration relative to today could push Earth into a moist-greenhouse state (assuming a fully saturated atmosphere). By contrast, the maximum destabilization occurred at 1000 times the present CO_2 level in Kasting et al. (1993). At larger pCO_2 values the increase in surface pressure outstrips the increase in the saturation vapor pressure of water, so the atmosphere becomes more stable against water loss (Kasting & Ackerman 1986). We conclude that planets with few tenths of a bar of pCO_2 have narrower HZs than planets like Earth on which pCO_2 is maintained at lower values by the carbonate-silicate cycle.

4. HABITABLE ZONES AROUND MAIN-SEQUENCE STARS

The procedure described in the previous section to derive HZs around the Sun can be used to estimate HZ boundaries around stars of different spectral types. A similar analysis was done by Kasting et al. (1993) for three stellar effective temperatures (7200, 5700, and 3700 K), which correspond to F0, G0, and M0 spectral types. Selsis et al. (2007b) used a similar model to that of Kasting et al. (1993) and interpolated HZ distances to stars within this range of effective temperatures. Here we compare our updated model results with these earlier studies and also extend the calculations to lower stellar effective temperatures to include M dwarfs. Correctly calculating HZs of M dwarfs is becoming increasingly important, as upcoming instruments such as Penn State's stabilized fiber-fed NIR spectrograph Habitable Zone Planet Finder (HPF; Mahadevan et al. 2012) and proposed missions such as *Transiting Exoplanet Survey Satellite* (*TESS*) will specifically search for low-mass planets around M dwarfs. Furthermore, several rocky planets have already been found in the HZs of M dwarfs (Bonfils et al. 2011; Vogt et al. 2012), and these objects may be good candidates for space-based characterization missions such as *JWST*.

4.1. Habitable Zone Boundaries around F, G, K, and M Stars

We considered stellar effective temperatures in the range $2600 \text{ K} \leqslant T_{\text{eff}} \leqslant 7200 \text{ K}$, which encompasses F, G, K, and M main-sequence spectral types. As input spectra for the HZ

boundary calculations we used the "BT_Settl" grid of models[17] (Allard et al. 2003, 2007). These cover the needed wavelength range for climate models (0.23–4.54 μm), as well as the range of effective temperatures (2600 K $\leqslant T_{\text{eff}} \leqslant$ 70,000 K) and metallicities ([Fe/H] −4.0 to +0.5) needed to simulate stellar spectra. Our comparison of the BT_Settl models with low-resolution IRTF data, and also high-resolution CRIRES data on Barnard's star (from the CRIRES_POP library[18] (Lebzelter et al. 2012)), show that the models are quite good in reproducing the gross spectral features and energy distributions of stars and will provide adequate input for our HZ calculations. For each star, the total energy flux over our climate model's spectral bands is normalized to 1360 W m^{-2} (the present solar constant for Earth) to simplify intercomparison.

In Figure 6, we compare the results of our inner and outer edge HZ model calculations for the Sun to stars of different spectral types. Unless otherwise specified, we use the HITEMP 2010 database for our inner edge calculations. The planetary albedo, shown in Figure 6(a) (inner edge) and Figure 6(c) (outer edge), of an Earth-like planet is higher if the host star is an F star and lower if its primary is an M star. The reason is that the Rayleigh scattering cross section (which is proportional to $1/\lambda^4$) is on average higher for a planet around an F star, as the star's Wien peak is bluer compared to the Sun. Second, H_2O and CO_2 have stronger absorption coefficients in the NIR than in the visible, so the amount of starlight absorbed by the planet's atmosphere increases as the radiation is redder (as is the case for an M star). Both effects are more pronounced when the atmosphere is dense and full of gaseous absorbers. For a late M star ($T_{\text{eff}} = 2600$ K) most of its radiation is peaked around 1 m. Therefore, the minimal amount of Rayleigh scattering and the high NIR absorption by the planet's atmosphere combine to generate extremely low planetary albedos.

The changes in predicted planetary albedo can be translated into critical solar fluxes, as shown in Figures 6(b) (inner edge) and (d) (outer edge). As discussed in Section 3.3, S_{eff} goes through a minimum near the OHZ because the atmosphere becomes optically thick at all IR wavelengths and, at the same time, the Rayleigh scattering due to CO_2 condensation increases planetary albedo. Note that for a late M star ($T_{\text{eff}} = 2600$ K) Rayleigh scattering never becomes an important factor, and hence S_{eff} asymptotically reaches a constant value. The parameter S_{eff} is directly calculated from our climate model and is dependent on the type of star considered. Therefore, we have derived relationships between HZ stellar fluxes (S_{eff}) reaching the top of the atmosphere of an Earth-like planet and stellar effective temperatures (T_{eff}) applicable in the range $2600 \text{ K} \leqslant T_{\text{eff}} \leqslant 7200 \text{ K}$:

$$S_{\text{eff}} = S_{\text{eff}\odot} + aT_{\star} + bT_{\star}^2 + cT_{\star}^3 + dT_{\star}^4, \qquad (2)$$

where $T_{\star} = T_{\text{eff}} - 5780$ K and the coefficients are listed in Table 3 for various habitability limits.[19] The corresponding HZ distances can be calculated using the relation

$$d = \left(\frac{L/L_\odot}{S_{\text{eff}}} \right)^{0.5} \text{AU}, \qquad (3)$$

where $L/L_\odot$ is the luminosity of the star compared to the Sun.

---

[17] http://perso.ens-lyon.fr/france.allard/
[18] http://www.univie.ac.at/crirespop/
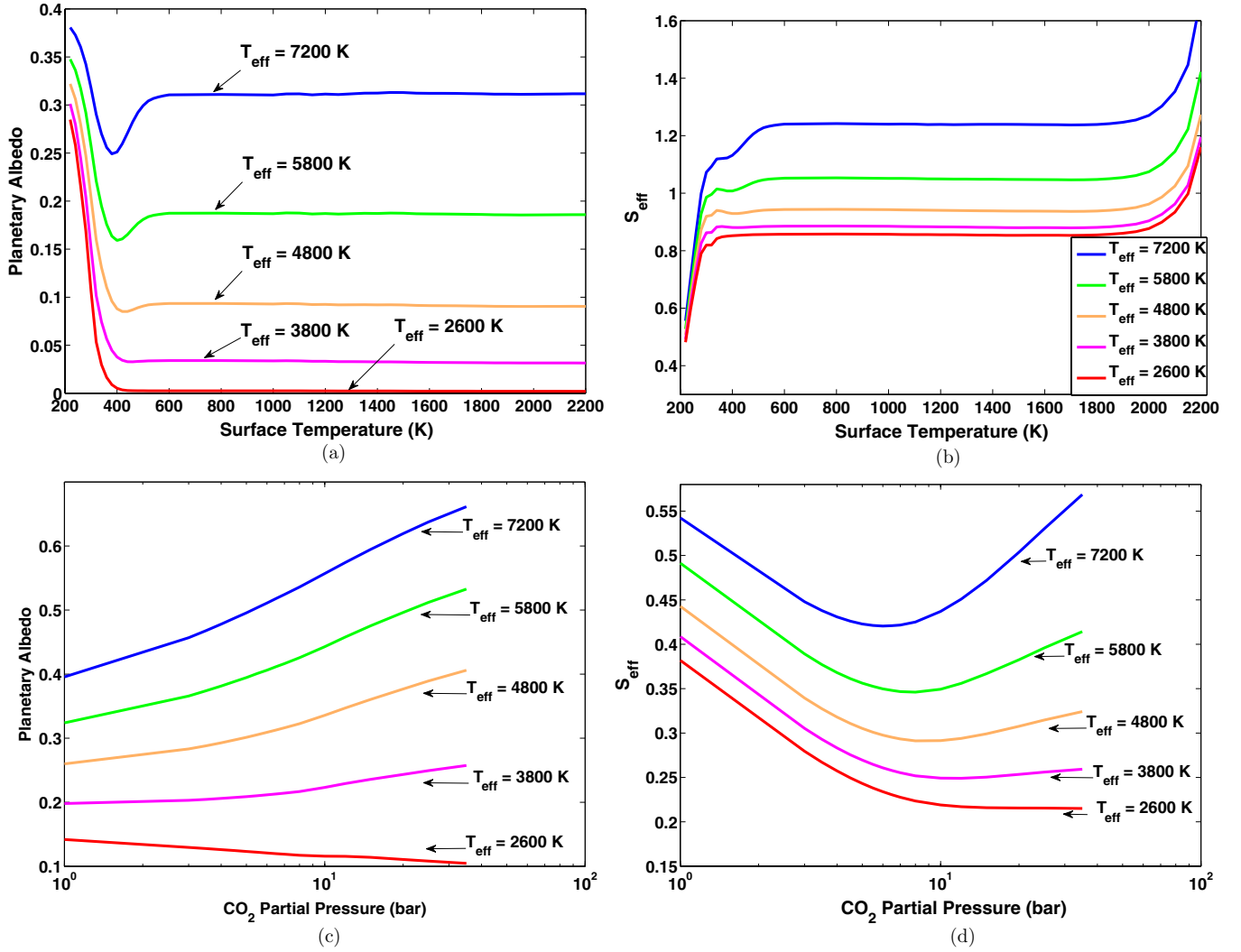[19] A FORTRAN code is also available to calculate HZ stellar fluxes.

Figure 6. Habitable zone calculations from our climate model for stellar effective temperatures corresponding to F ($T_{eff} = 7200$ K), G (Sun), K ($T_{eff} = 4800$ K), and M ($T_{eff} = 3800$ K and 2600 K) spectral types. The inner edge results are shown in (a) and (b), and the outer edge results are shown in (c) and (d).

(A color version of this figure is available in the online journal.)

Table 3
Coefficients to Be Used in Equation (2) to Calculate Habitable Stellar Fluxes, and Corresponding Habitable
Zones (Equation (3)), for Stars with $2600\,\text{K} \leqslant T_{eff} \leqslant 7200\,\text{K}$

Constant	Recent Venus	Runaway Greenhouse	Moist Greenhouse	Maximum Greenhouse	Early Mars
$S_{eff\odot}$	1.7753	1.0512	1.0140	0.3438	0.3179
a	1.4316×10^{-4}	1.3242×10^{-4}	8.1774×10^{-5}	5.8942×10^{-5}	5.4513×10^{-5}
b	2.9875×10^{-9}	1.5418×10^{-8}	1.7063×10^{-9}	1.6558×10^{-9}	1.5313×10^{-9}
c	-7.5702×10^{-12}	-7.9895×10^{-12}	-4.3241×10^{-12}	-3.0045×10^{-12}	-2.7786×10^{-12}
d	-1.1635×10^{-15}	-1.8328×10^{-15}	-6.6462×10^{-16}	-5.2983×10^{-16}	-4.8997×10^{-16}

In Figure 7, we compare HZ fluxes (and distances) calculated using Equations (2) and (3) for the moist-greenhouse case, with Selsis et al. (2007b) 0% cloud results for different stellar effective temperatures. As shown in Figure 7(a), for low T_{eff}, there are large differences at the inner edge (dashed and solid red curves) between the models. This is because the spectrum of low-mass stars shifts toward the longer wavelengths, resulting in more NIR flux compared to high-mass stars. In both the models the atmosphere of a planet in the inner HZ is H_2O dominated, and so there is strong absorption in the NIR. Since our model uses the most recent HITEMP database, which has more H_2O lines in the NIR, the moist-greenhouse limit occurs at a lower

flux (farther from the star). Also, Selsis et al. (2007b) assumed $T_{eff} = 3700$ K for stars with temperatures below this value. This amplifies the differences, as these low-mass stars have their peak fluxes in NIR. These differences in inner HZ boundaries may become important for present and upcoming planet-finding surveys around M dwarfs such as MEARTH (Nutzman & Charbonneau 2008) and Penn State's HPF (Mahadevan et al. 2012), whose goal is to discover potentially habitable planets around M dwarfs.

The luminosity of a main-sequence star evolves over time, and consequently the HZ distances (Equation (3)) also change with time. One can calculate "continuous" HZ (CHZ) boundaries
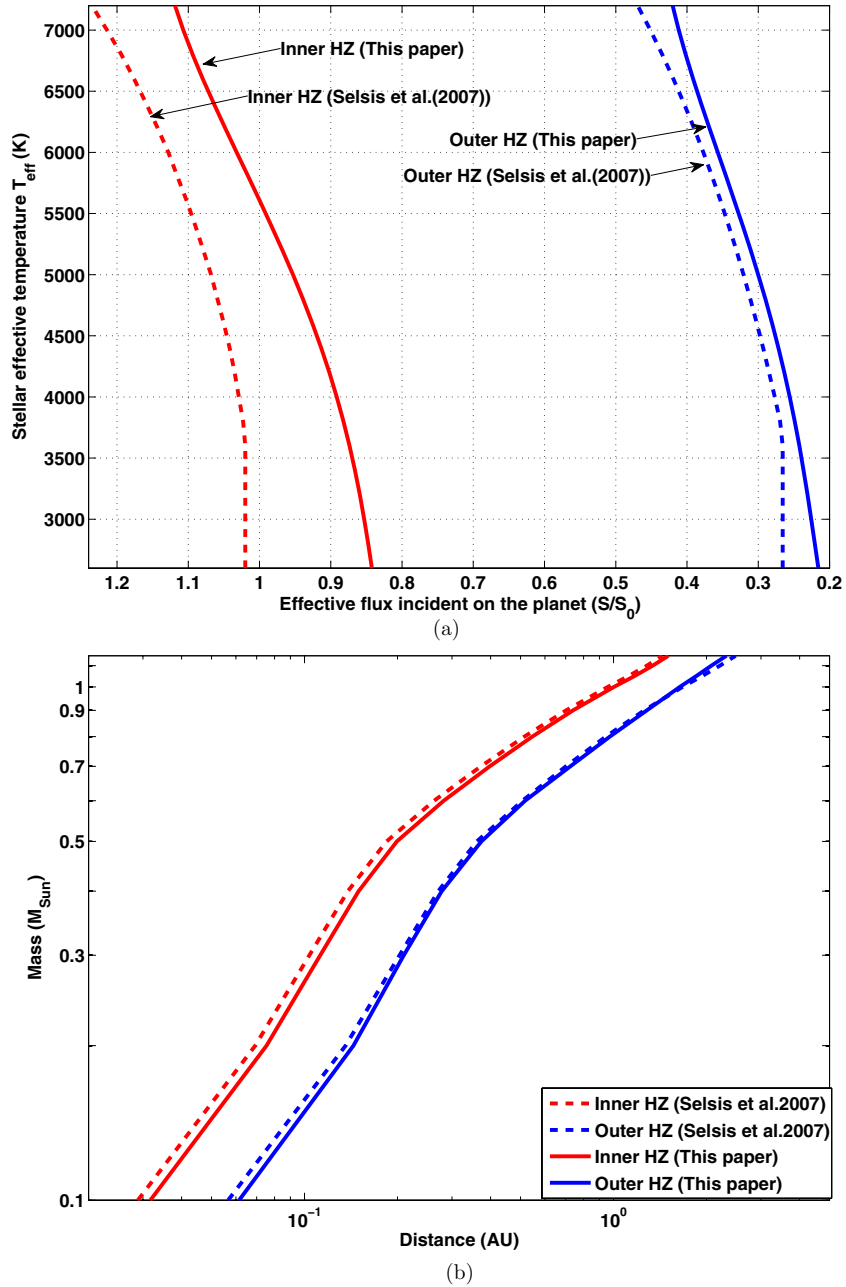
Figure 7. Habitable zone fluxes (panel (a)) and corresponding distances (panel (b)) from our model (solid lines) compared to Selsis et al. (2007b) results (dashed lines) for different stellar effective temperatures. The inner HZ fluxes from our model (red solid lines) are for the moist-greenhouse case, and outer edge fluxes (blue solid lines) are for the maximum greenhouse limit, which are compared with 0% cloud cover limit from Table 2 of Selsis et al. (2007b). The corresponding continuous HZ distances for 5 Gyr are shown in panel (b).

(A color version of this figure is available in the online journal.)

within which a planet remains habitable for a specified length of time (we chose 5 Gyr). In Figure 7(b), we show CHZ boundaries as a function of stellar mass for both our model and the Selsis et al. (2007b) model, taking into account the stellar evolutionary models of Baraffe et al. (1998) for solar-metallicity stars. Noticeable differences between the two models are seen for low-mass stars near the inner edge (as also seen in Figure 7(a)). The large differences in S_{eff} from Figure 7(a) do not appear as pronounced in Figure 7(b) because it is a log scale and also because the CHZ distance is inversely proportional to the square root of S_{eff} (Equation (3)).

In order to assess the potential habitability of recently discovered exoplanets, equilibrium temperature (T_{eq}) has been

used as a metric (Borucki et al. 2011; Batalha et al. 2012). Assuming an emissivity of 0.9, the ranges of HZ boundaries are taken to be $185 \text{ K} \leqslant T_{eq} \leqslant 303 \text{ K}$ (Kasting 2011). We would like to stress that the stellar fluxes (S_{eff}) provide a better metric for habitability than does T_{eq}. This is because T_{eq} involves an assumption about A_B (0.3, usually) that is generally not valid. This value of A_B is good for present Earth around our Sun. For a planet around a late M star, A_B can vary from 0.01 near the inner edge to 0.1 at the outer edge (see Figure 6), depending on its location. Similarly, A_B for an F star can range in between 0.38 and 0.51 for the inner and outer edge, respectively. This changes the corresponding T_{eq}, and so a uniform criterion for HZ boundaries based on T_{eq} cannot be determined.
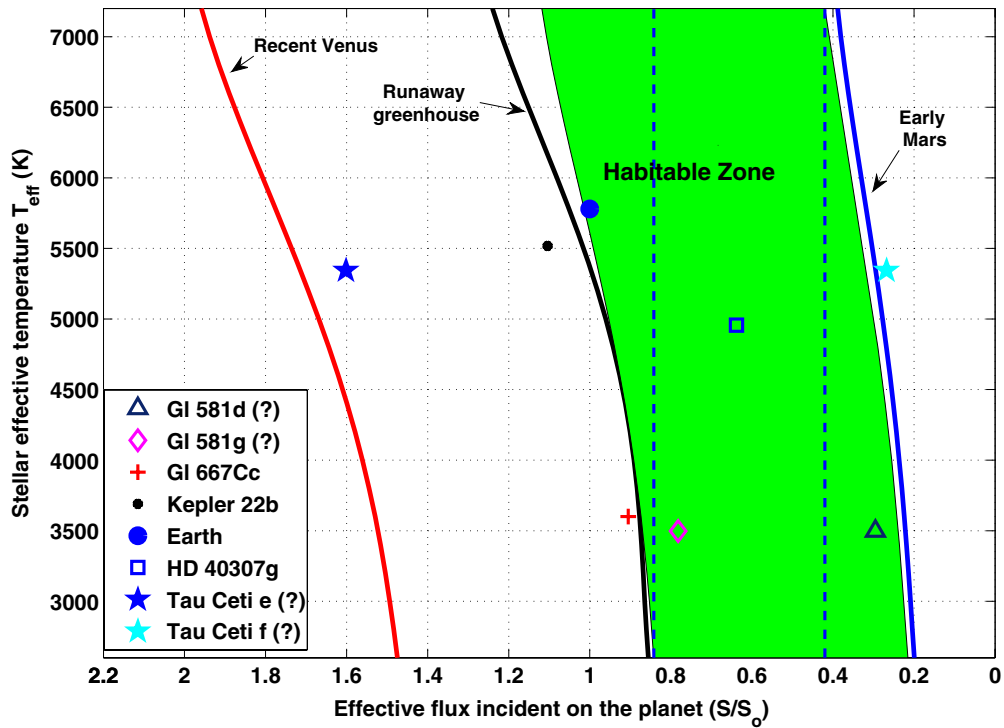
Figure 8. Various cloud-free habitable zone (flux) boundaries for stars with different T_{eff}. The boundaries of the green shaded region are determined by the moist greenhouse (inner edge, higher flux values) and the maximum greenhouse (outer edge, lower flux values). A planet that receives stellar flux bounded by the two dashed vertical lines is in the HZ irrespective of the stellar type. Some of the currently known exoplanets that are thought to be in the HZ by previous studies are also shown. The "?" for the Gl 581 and Tau Ceti system of planets imply that there is an ongoing discussion about their existence. For stars with $T_{eff} \lesssim 5000$ K, there is no clear distinction between runaway and moist-greenhouse limit.

(A color version of this figure is available in the online journal.)
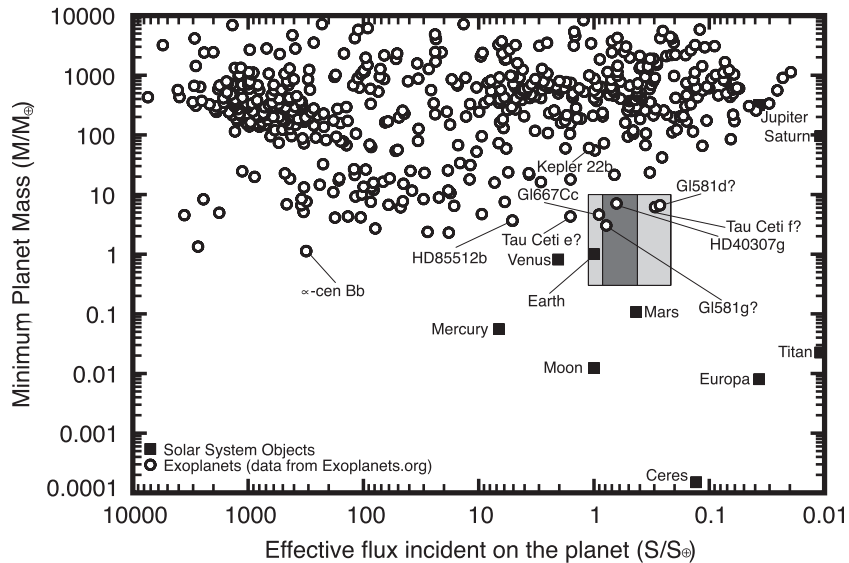
Figure 9. HZ boundaries combining observable stellar and planetary parameters. Terrestrial planets (0.3–10 $M_{\oplus}$, y-axis limits) within the dark shaded region are in the HZ irrespective of the stellar type. For those planets in the light gray region, one needs to know the stellar type to determine if they are in the HZ. For example, the Earth would not be habitable if it received its current incoming amount of energy from a cooler-type star, but it is (obviously) habitable in its current orbit around a G-type star. For planets such as this, the star's energy distribution matters when considering habitability.

5. DISCUSSION

A straightforward application of the calculations presented in the previous sections is to apply them to currently known exoplanetary systems. Figure 8 shows various HZ boundaries (expressed in terms of effective stellar flux) as a function of stellar T_{eff}. The orbital parameters of the planets and stellar characteristics were obtained from exoplanets.org (Wright et al. 2011). The green-shaded habitable region is bounded by the moist-greenhouse limit (inner edge) and the maximum green-house limit (outer edge). Several currently known terrestrial mass exoplanets that have been proposed to be in the HZ by various studies are also shown. An important insight that can be obtained from this figure (and one that cannot be seen in the

HZ distance plot, Figure 7(b)) is that a terrestrial mass planet that lies within the two vertical dashed lines in the green shaded region is in the HZ irrespective of the type of star it is orbiting. The corresponding flux boundaries for which a rocky planet is "definitely" in the HZ are 0.842 and 0.42. Currently, two exoplanets fall within this region, HD 40307g (Tuomi et al. 2012) and Gl 581g (Vogt et al. 2010, 2012). The detection of planets and orbital parameters for Gl581 is complicated by the low amplitudes of the signal, stellar activity, and possible red noise. We have included a "?" for the Gl 581 system of planets in the plot, indicating that there is an active ongoing discussion in the literature about the number of planets in this system and their exact orbital parameters (Vogt et al. 2010; Pepe et al. 2011b; Vogt et al. 2012; Baluev 2013). Furthermore, for stars with $T_{\rm eff} \lesssim 5000$ K, there is no clear distinction between runaway greenhouse and the moist-greenhouse limits. The reason is that for these stars, there are more photons available in the IR part of the spectrum, where H_2O is a good absorber. Therefore, a planet with H_2O-dominated atmosphere quickly goes into runaway once it reaches the moist-greenhouse limit. Note that another suggested HZ candidate planet, HD 85512b (Pepe et al. 2011a), receives more than five times the stellar flux received by our Earth, placing it even beyond the most liberal ("recent Venus") estimate of the inner edge. Hence, it is very likely that this planet is not in the HZ of its star.

A question of importance to the exoplanet community is which HZ limits to choose when identifying potentially habitable planets. For current RV surveys and *Kepler* mission, one should use the most conservative limits (moist greenhouse and maximum greenhouse) because this will give a lower limit on $\eta_\oplus$, the fraction of Sun-like stars that have at least one planet in the HZ (Lunine et al. 2008). If one is interested in designing a future flagship mission, such as *Terrestrial Planet Finder* (*TPF*) or *Darwin*, then using these conservative limits (which results in a lower limit on $\eta_\oplus$) ensures that the telescope is not undersized. If, however, one was analyzing data obtained from such a telescope, the most optimistic limits (recent Venus and early Mars) should be used because one would not want to miss out on any potentially habitable planets.

In Figure 9, we show the incident stellar flux as a function of planetary mass for the currently known exoplanets. The masses are obtained from exoplanets.org when available. Also shown are HZ flux boundaries calculated from Equation (2) for terrestrial mass planets (1 $M_\oplus$–10 $M_\oplus$). For the outer box (light gray), the upper bound on the flux is taken to be the moist-greenhouse limit for a star with $T_{\rm eff} = 7200$ K, and the lower bound is the maximum greenhouse limit for a star with $T_{\rm eff} = 2600$ K. These are indicated by the diagonally opposite points on the green shaded region in Figure 8. For the inner box (dark gray), the flux limits are the dashed lines in the green shaded region of Figure 8. The significance of this plot is that terrestrial planets in the inner box must be in the HZ, irrespective of the stellar spectral type. Mars, if it were more massive, would be in the HZ around any main-sequence star with $2600 \leqslant T_{\rm eff} \leqslant 7200$ K. For planets that are outside the dark gray region, but inside the light gray (for example, Earth), one needs to know the host star's spectral type (or $T_{\rm eff}$) to determine if that planet is in the HZ. Figure 9 combines observable stellar and planetary parameters to further constrain HZ boundaries for extrasolar planets.

Many of the currently known exoplanets have non-zero eccentricities, which can carry some of them (and their possible moons) in and out of the HZ. The incident stellar flux on these

eccentric planets has extreme variations between periastron and apoastron ($[(1 + e)/(1 - e)]^2$). Williams & Pollard (2002) show that, provided that an ocean is present to act as a heat capacitor, it is primarily the time-averaged flux $\langle S'_{\rm eff} \rangle$ that affects the habitability over an eccentric orbit. Mathematically

$$\langle S'_{\rm eff} \rangle = \frac{S_{\rm eff}}{(1 - e^2)^{1/2}}. \qquad (4)$$

Here $S_{\rm eff}$ is the effective flux from circular orbit (Equation (2)). Planets with high orbital eccentricities ($e \gtrsim 0.1$) have higher average orbital flux. This may help eccentric planets near the OHZ maintain habitable conditions.

Earth itself appears to be perilously close to the moist-greenhouse limit ($S_{\rm eff} = 1.015$, blue filled circle in Figure 8). However, this apparent instability is deceptive, because the calculations do not take into account the likely increase in Earth's albedo that would be caused by water clouds on a warmer Earth. Furthermore, these calculations assume a fully saturated troposphere that maximizes the greenhouse effect. For both reasons, it is likely that the actual HZ inner edge is closer to the Sun than our moist-greenhouse limit indicates. Note that the moist greenhouse in our model occurs at a surface temperature of 340 K. The current average surface temperature of the Earth is only 288 K. Even a modest (5°–10°) increase in the current surface temperature could have devastating effects on the habitability of Earth from a human standpoint. Consequently, though we identify the moist-greenhouse limit as the inner edge of the HZ, habitable conditions for humans could disappear well before Earth reaches this limit.

Additional uncertainty about habitability of planets around late K and M stars ($T_{\rm eff} \leqslant 4000$ K) comes from the fact that planets within the HZs of these stars are expected to be tidally locked (Dole 1964; Peale 1977; Kasting et al. 1993; Dobrovolskis 2009). If the planet's orbital eccentricity is small, this can result in synchronous rotation, in which one side of a planet always faces the star (as the Moon does to the Earth). Climates of synchronously rotating planets are not well approximated by 1D, globally averaged models. Previous work has shown that such planets may indeed be habitable (Joshi et al. 1997; Joshi 2003; Edson et al. 2003); however, systematic exploration of synchronously rotating planets in different parts of the HZ has not been attempted. Even before doing these calculations, we can predict that planets near the OHZ, with their expected dense CO_2 atmospheres, should be more effective at transporting heat around to their night sides and hence should have a better chance of being habitable.

Given that surveys such as HPF and CARMENES will specifically target mid- to late M dwarfs, our future work will include estimating the HZ boundaries of individual targets in detail. Ongoing work by our team (Terrien et al. 2012) is yielding low-resolution NIR spectra from the Infrared Telescope Facility (IRTF) to be used to derive stellar metallicities, as well as yielding more realistic flux distributions and temperatures for use in the modeling. We anticipate having this information for ∼650 M dwarfs drawn from the $J < 10$ Lepine & Gaidos (2011) catalog and have applied for time to observe ∼300 more. Estimates of luminosities will be derived using photometric and spectroscopic distances for now (in cases where parallax measurements are absent), but eventually *Gaia* (Perryman et al. 2001) will yield very precise parallaxes (and by extension precise luminosities) for all these target stars.

Recent discoveries by both the *Kepler* mission and RV surveys have shown that planets can exist in stable orbits around

multiple-star systems (Doyle et al. 2011; Welsh et al. 2012; Orosz et al. 2012; Dumusque et al. 2012). The HZs of these stars could potentially host terrestrial planets, which are at the threshold of current detection techniques. Indeed, the discovery of Kepler 47c (Orosz et al. 2012), which is 4.6 times the size of Earth's radii in the HZ, is a step closer to discovering rocky planets in the HZ of multiple-star systems. Dumusque et al. (2012) have recently published a possible detection of a 1.1 Earth mass (minimum) planet in a 3.236 day orbit around the α Centauri system. So, this system should now be a prime target for further observations to discover habitable planets. Formation of dynamically stable terrestrial planets in the HZs of multiple-star systems has been studied before (Whitmire et al. 1998; Holman & Wiegert 1999; Haghighipour & Raymond 2007), and several studies estimated HZ boundaries around these types of systems (Eggl et al. 2012, 2013; Kane & Hinkel 2013) using the Kasting et al. (1993) model. Our updated model results from Figure 8 or Equations (2) and (3) could change these estimates significantly.

Our new model results could also directly affect estimates of $\eta_\oplus$. Recent analysis of *Kepler* data (Traub 2012) and RV surveys (Bonfils et al. 2011) concluded that $\eta_\oplus \sim 0.34$–0.4. These values were based on either the Kasting et al. (1993) model (Traub 2012) or the Selsis et al. (2007b) results (Bonfils et al. 2011). Our new HZ limits could impact these estimates significantly. In particular, there are large differences between Selsis et al. (2007b) calculations and our model results for low-mass stars. The estimate of $\eta_\oplus$ by Bonfils et al. (2011) is obtained by using Selsis et al. (2007b) relationships for planets orbiting M stars. Thus, this value may need to be re-evaluated.

6. CONCLUSIONS

We have obtained new estimates for HZs around F, G, K, and M main-sequence stars by (1) updating H_2O and CO_2 absorption coefficients in the Kasting et al. (1993) 1D radiative–convective, cloud-free climate model with the most recent LBL databases: HITRAN 2008 and HITEMP 2010; (2) correcting the H_2O Rayleigh scattering coefficient; and (3) updating CO_2 collision-induced absorption coefficients. These changes affect the inner and outer edges of the HZ, respectively.

Our revised model predicts that the moist-greenhouse limit for our Sun, which defines the inner edge of the HZ, is at 0.99 AU. The OHZ, where gaseous CO_2 produces its maximum greenhouse effect, is at 1.70 AU. Although it appears that Earth is perilously close to the inner HZ edge, in reality, cloud feedback and low upper tropospheric relative humidity act to stabilize Earth's climate. Theoretical studies and observational surveys that depend on these limits should use the updated values. We have also estimated HZ boundaries for M stars with $T_{\rm eff}$ as low as 2600 K, which are primary targets for ongoing surveys such as HPF and MEARTH to discover potential habitable planets.

We also showed that the effective stellar flux provides a better criterion in determining the HZ limits than equilibrium temperature. Accordingly, we have derived a generalized expression to calculate these fluxes for stars of different spectral types. Our results show that some of the extrasolar planets that were previously thought to be within the HZ may not be in that region. Thus, our HZ estimates can be used to narrow the target list for eventual characterization missions, such as *JWST*, to identify potential biomarkers on habitable planets.

Author Contribution: R.K. and R.R. contributed equally to this work. An interactive Web page to obtain HZs and a FOR-TRAN code is available at http://depts.washington.edu/naivpl/ content/hz-calculator. The FORTRAN code is also available in the electronic version of the paper.

REFERENCES

Abe, Y., Abe-Ouchi, A., Sleep, N. H., & Zahnle, K. J. 2011, AsBio, 11, 443
Allard, F., Allard, N. F., Homeier, D., et al. 2007, A&A, 474, L21
Allard, F., Guillot, T., Ludwig, H. G., et al. 2003, in IAU Symp. 211, Brown Dwarfs, ed. E. Martín (San Francisco, CA: ASP), 325
Allen, C. 1976, Astrophysical Quantities (London: Athlone)
Bahcall, J. N., Pinsonneault, M. H., & Basu, S. 2001, ApJ, 555, 990
Baluev, R. V. 2013, MNRAS, 429, 2052
Baraffe, I., Chabrier, G., Allard, F., & Hauschildt, P. 1998, A&A, 337, 403
Baranov, Y. I., Lafferty, W. J., & Fraser, G. T. 2004, JMoSp, 228, 432
Batalha, N. M., Rowe, J. F., Bryson, S. T., et al. 2012, ApJS, submitted (arXiv:1202.5852)
Bezard, B., Debergh, C., Crisp, D., & Maillard, J. P. 1990, Natur, 345, 508
Bibring, J.-P., Langevin, Y., Mustard, J. F., et al. 2006, Sci, 312, 400
Bonfils, X., Delfosse, X., Udry, S., et al. 2011, A&A, submitted (arXiv:1111.5019)
Borucki, W. J., Koch, D. G., Basri, G., et al. 2011, ApJ, 736, 19
Borucki, W. J., Koch, D. G., Batalha, N., et al. 2012, ApJ, 745, 120
Bucholtz, A. 1995, ApOpt, 34, 2765
Burch, D. E., Gryvnak, D. A., Patty, R. R., & Bartky, C. E. 1969, JOSA, 59, 267
Clampin, M., Valenti, J., & Deming, D. 2007, Detection of Planetary Transits with the James Webb Space Telescope. ExoPTF Whitepaper
Clough, S. A., & Iacono, M. J. 1995, JGR, 100, 16519
Clough, S. A., Kneizys, F. X., & Davies, R. W. 1989, AtmRe, 23, 229
Colaprete, A., & Toon, O. B. 2003, JGRE, 108, 6
Crisp, D. 1997, GeoRL, 24, 571
Deming, D., Seager, S., Winn, J., et al. 2009, PASP, 121, 952

Dobrovolskis, A. R. 2009, Icar, 204, 1
Dole, S. H. 1964, Habitable Planets for Man (New York: Blaisdell Publishing), 158
Doyle, L. R., Carter, J. A., Fabrucky, D. C., et al. 2011, Sci, 333, 1602
Dumusque, X., Francesco, P., Christophe, L., et al. 2012, Natur, 491, 207
Edlén, B. 1966, Metro, 2, 71
Edson, A., Lee, S., Bannon, P., Kasting, J. F., & Pollard, D. 2011, Icar, 212, 1
Eggl, S., Pilat-Lohinger, E., & Funk, B. 2013, MNRAS, 428, 3104
Eggl, S., Pilat-Lohinger, E., Georgakarakos, N., et al. 2012, ApJ, 752, 74
Forget, F., & Pierrehumbert, R. T. 1997, Sci, 278, 1273
Forget, F., Wordsworth, R. W., Millour, E., et al. 2013, Icar, 222, 81
Fukabori, M., Nakazawa, T., & Tanaka, M. 1986, JQSRT, 36, 265
Goldblatt, C., & Zahnle, K. 2011, Natur, 474, 7349
Gough, D. O. 1981, SoPh, 74, 21
Gruszka, M., & Borysow, A. 1997, Icar, 129, 172
Haghighipour, N., & Raymond, S. 2007, ApJ, 666, 436
Halevy, I., Pierrehumbert, R. T., & Schrag, D. P. 2009, JGR, 114, D18112
Haqq-Misra, J. D., Domagal-Goldman, S. D., Kasting, P. J., & Kasting, J. F. 2008, AsBio, 8, 1127
Hart, M. H. 1978, Icar, 33, 23
Holman, M. J., & Wiegert, P. A. 1999, AJ, 117, 621
Huang, S. S. 1959, AmSci, 47, 397
Joshi, M. M. 2003, AsBio, 3, 415
Joshi, M. M., Haberle, R. M., & Reynolds, R. T. 1997, Icar, 129, 450
Kaltenegger, L., & Sasselov, D. 2011, ApJL, 736, L25
Kaltenegger, L., Segura, A., & Mohanty, S. 2011, ApJ, 733, 35
Kaltenegger, L., & Traub, W. 2009, ApJ, 698, 519
Kane, S. R., & Hinkel, N. R. 2013, ApJ, 762, 7
Kasting, J. F. 1988, Icar, 74, 472
Kasting, J. F. 1991, Icar, 94, 1
Kasting, J. F. 2011, Joint Meeting of the Exoplanet and Cosmic Origins Program Analysis Groups (ExoPAG and COPAG), 2011 April 26, Baltimore, MD, http://exep.jpl.nasa.gov/exopag/exopagCopagJointMeeting/
Kasting, J. F., & Ackerman, T. P. 1986, Sci, 234, 1383
Kasting, J. F., Pollack, J. B., & Crisp, D. 1984, JAtC, 1, 403
Kasting, J. F., Whitmire, D. P., & Reynolds, R. T. 1993, Icar, 101, 108
Kato, S., Ackerman, T. P., Mather, J. H., et al. 1999, JQSRT, 62, 109
Kitzmann, D., Patzer, A. B. C., Von Paris, P., Godolt, M., & Rauer, M. 2011a, A&A, 531, A62
Kitzmann, D., Patzer, A. B. C., Von Paris, P., Godolt, M., & Rauer, M. 2011b, A&A, 534, A63
Lebzelter, T., Seifahrt, A., Uttenthaler, S., et al. 2012, A&A, 539, 25
Lepine, S., & Gaidos, E. 2011, AJ, 142, 15
Lunine, J. I., Fischer, D., Hammel, H. B., et al. 2008, AsBio, 8, 875
Mahadevan, S., Ramsey, L., Bender, C., et al. 2012, Proc. SPIE, 8446, 84461S
Marshall, B. R., & Smith, R. C. 1990, ApOpt, 29, 71
Meadows, V. S., & Crisp, D. 1996, JGR, 101, 4595
Mischna, M. A., Kasting, J. F., Pavlov, A., & Freedman, R. 2000, Icar, 145, 546
Mlawer, E. J., Taubman, S. J., Brown, P. D., et al. 1997, JGR, 102, 16663
Nutzman, P., & Charbonneau, D. 2008, PASP, 120, 317

Orosz, J. A., Welsh, W. F., Carter, J. A., et al. 2012, Sci, 337, 1511
Paynter, D. J., & Ramaswamy, V. 2011, JGRD, 116, D20302
Peale, S. J. 1977, in Planetary Satellites, Rotational Histories of the Natural Satellites, ed. J. A. Burns (Tucson, AZ: Univ. Arizona Press)
Pepe, F., Lovis, C., Segransan, D., et al. 2011a, A&A, 534, A58
Pepe, F., Mayor, M., Lovis, C., et al. 2011b, in IAU Symp. 276, The Astrophysics of Planetary Systems: Formation, Structure, and Dynamical Evolution, ed. A. Sozzetti, M. G. Lattanzi, & A. P. Boss (Cambridge: Cambridge Univ. Press), 13
Perrin, M. Y., & Hartmann, J. M. 1989, JQSRT, 42, 311
Perryman, M. A. C., de Boer, K. S., Gilmore, G., et al. 2001, A&A, 369, 339
Pierrehumbert, R. T. 2010, Principles of Planetary Climate (Cambridge: Cambridge Univ. Press)
Pierrehumbert, R. T. 2011, ApJL, 726, L8
Pollack, J. B., Kasting, J. F., Richardson, S. M., & Poliakoff, K. 1987, Icar, 71, 203
Ramirez, R. M., Zugger, M. E., & Kasting, J. F. 2013, NatGe, submitted
Robinson, T., Meadows, V., Crisp, D., et al. 2011, AsBio, 11, 393
Rothman, L. S., Gordon, I. E., Barber, A., et al. 2008, JQSRT, 110, 533
Rothman, L. S., Gordon, I. E., Barber, A., et al. 2010, JQSRT, 111, 2139
Segura, T. L., Toon, O. B., & Colaprete, A. 2008, JGR, 113, E11007
Segura, T. L., Toon, O. B., Colaprete, A., & Zahnle, K. 2002, Sci, 298, 1977
Selsis, F., Chazelas, B., Bordé, P., et al. 2007a, Icar, 191, 453
Selsis, F., Kasting, J. F., Levrard, B., et al. 2007b, A&A, 476, 137
Shine, K. P., Ptashnik, I. V., & Radel, G. 2012, SGeo, 33, 535
Solomon, S. C., & Head, J. W. 1991, Sci, 252, 252
Sykes, J. B. 1952, MNRAS, 3, 377
Terrien, R. C., Mahadevan, S., Bender, C., et al. 2012, ApJL, 747, L38
Thomas, G. E., & Stamnes, K. 2002, Radiative Transfer in the Atmosphere and Ocean (Cambridge: Cambridge Univ. Press)
Tian, F., Claire, M. W., Haqq-Misra, J. D., et al. 2010, E&PSL, 295, 412
Toon, O. B., McKay, C. P., Ackerman, T. P., & Santhanam, K. 1989, JGR, 94, 16287
Traub, W. A. 2012, ApJ, 745, 20
Tuomi, M., Anglada-Escude, G., Gerlach, E., et al. 2012, A&A, 549, A48
Udry, S., Bonfils, X., Delfosse, X., et al. 2007, A&A, 469, L43
Underwood, D. R., Jones, B. W., & Sleep, P. N. 2003, IJAsB, 2, 289
Vardavas, I. M., & Carver, J. H. 1984, P&SS, 32, 1307
Vogt, S. S., Butler, P., & Haghighipour, N. 2012, AN, 333, 561
Vogt, S. S., Butler, R. P., Rivera, E. J., et al. 2010, ApJ, 723, 954
Von Paris, P., Gebauer, S., Godolt, M., Rauer, H., & Stracke, B. 2011, A&A, 532, A58
Von Paris, P., Gebauer, S., Godolt, M., et al. 2010, A&A, 522, A23
Welsh, W., Orosz, J. A., Carter, J. A., et al. 2012, Natur, 481, 475
Whitmire, D. P., Matese, J. J., & Criswell, L. 1998, Icar, 132, 196
Williams, D. M., & Pollard, D. 2002, IJAsB, 1, 61
Wordsworth, R., Forget, F., & Eyment, V. 2010, Icar, 210, 992
Wordsworth, R. D., Forget, F., Selsis, F., et al. 2011, ApJ, 733, L48
Wright, J. T., Fakhouri, O., Marcy, G. W., et al. 2011, PASP, 123, 412
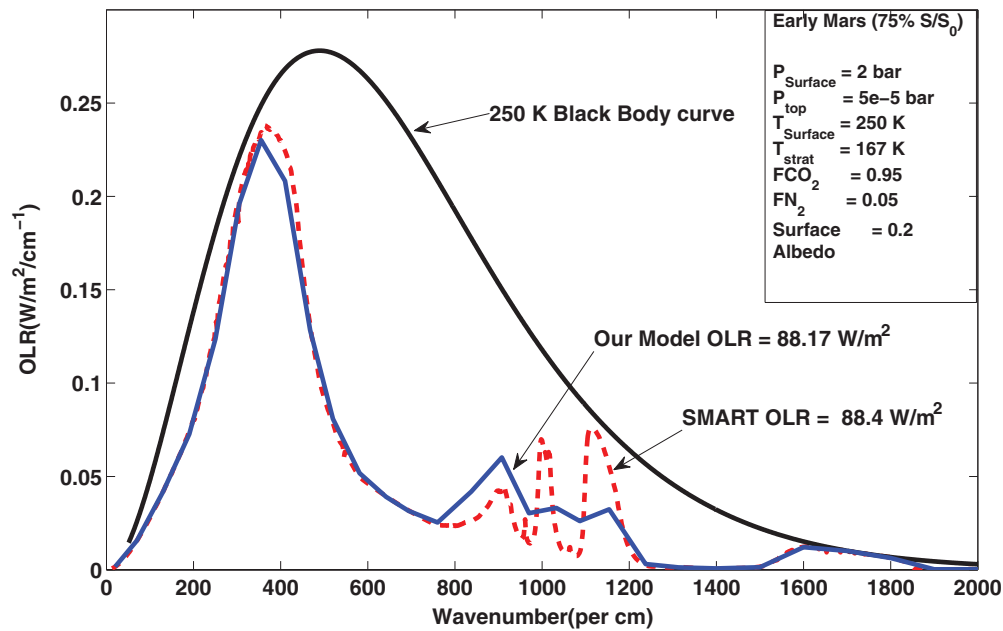Zsom, A., Kaltenegger, L., & Goldblatt, C. 2012, Icar, 221, 603

Figure 1. Plot of outgoing long-wave radiation vs. wavenumber for the 0–2000 cm^{-1} region comparing our OLR (blue solid curve) to that from SMART (red dashed curve). This calculation is for early Mars conditions, 2 bar CO_2, and constant stratospheric and surface temperatures of 167 and 250 K, respectively. The corresponding 250 K blackbody curve is shown in black. The integrated flux over all bands at the top of the atmosphere is 88.17 Wm^{-2} for our model and 88.4 Wm^{-2} for SMART.
(A color version of this figure is available in the online journal.)
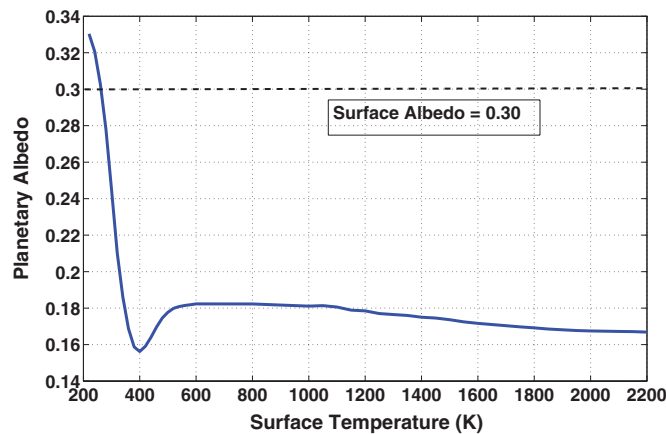
Figure 3. Inner edge of the habitable zone calculations from our updated climate model. Various parameters are shown as a function of surface temperature: (b) planetary albedo.
(A color version of this figure is available in the online journal.)

Table 1
Habitable Zone Distances around Our Sun from Our Updated 1D Climate Model

Model	Inner Habitable Zone			Outer Habitable Zone	
	Moist Greenhouse	Runaway Greenhouse	Recent Venus	Maximum Greenhouse	Early Mars
This paper	0.99 AU	0.97 AU	0.75 AU	1.67 AU	1.77 AU
Kasting et al. (1993)	0.95 AU	0.84 AU	0.75 AU	1.67 AU	1.77 AU

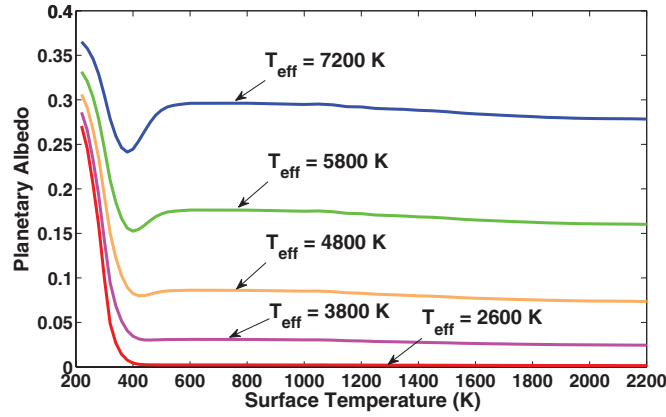**Note.** For comparison, estimates from Kasting et al. (1993) are also shown.

Figure 6. Habitable zone calculations from our climate model for stellar effective temperatures corrresponding to F ($T_{eff} = 7200$ K), G (Sun), K ($T_{eff} = 4800$ K), and M ($T_{eff} = 3800$ K, and 2600 K) spectral types. The inner edge results are shown in (a).

(A color version of this figure is available in the online journal.)

Table 3
Updated Coefficients to Calculate Habitable Stellar Fluxes, and Corresponding Habitable Zones, for Stars with $2600 \leqslant T_{eff} \leqslant 7200$ K

Constant	Recent Venus	Runaway Greenhouse	Moist Greenhouse	Maximum Greenhouse	Early Mars
$S_{eff\odot}$	1.7763	1.0385	1.0146	0.3507	0.3207
a	1.4335×10^{-4}	1.2456×10^{-4}	8.1884×10^{-5}	5.9578×10^{-5}	5.4471×10^{-5}
b	3.3954×10^{-9}	1.4612×10^{-8}	1.9394×10^{-9}	1.6707×10^{-9}	1.5275×10^{-9}
c	-7.6364×10^{-12}	-7.6345×10^{-12}	-4.3618×10^{-12}	-3.0058×10^{-12}	-2.1709×10^{-12}
d	-1.1950×10^{-15}	-1.7511×10^{-15}	-6.8260×10^{-16}	-5.1925×10^{-16}	-3.8282×10^{-16}

Note. An ASCII file containing these coefficients can be downloaded in the electronic version of the journal.

Note added in proof. R. Wordsworth pointed out that his model uses increased vertical resolution in the lower atmosphere and that his results were found to be insensitive to further increases in resolution. All such calculations should be tested to determine whether they are robust to this issue.

REFERENCES

Abbot, D. S., Cowan, N. B., & Ciesla, F. J. 2012, ApJ, 756, 178
Bucholtz, A. 1995, ApOpt, 34, 2765
Dressing, C. D., Spiegel, D. S., Scharf, C. A., Menou, K., & Raymond, S. N. 2010, ApJ, 721, 1295
Edlén, B. 1966, Metro, 2, 71
Kasting, J. F., Whitmire, D. P., & Reynolds, R. T. 1993, Icar, 101, 108
Kopparapu, R., & Barnes, R. 2010, ApJ, 716, 1336
Kopparapu, R., Raymond, S. N., & Barnes, R. 2009, ApJL, 695, L181
Marshall, B. R., & Smith, R. C. 1990, ApOpt, 29, 71
Spiegel, D. S., Menou, K., & Scharf, C. A. 2008, ApJ, 681, 1609
Spiegel, D. S., Menou, K., & Scharf, C. A. 2009, ApJ, 691, 596
Von Paris, P., Gebauer, S., Godolt, M., et al. 2010, A&A, 522, A23